Evaluation of low permeability conglomerate reservoirs based on petrophysical facies: A case study from the Triassic Baikouquan Formation, northern Mahu Sag, Junggar Basin, China

Zhichao Yu [a], Zhizhang Wang [a,*], Qingping Jiang [b], Jie Wang [c], Yueli Feng [b], Jingrong Zheng [a], Bestman Adjei Baffour [a]

[a] College of Geosciences, China University of Petroleum, Beijing, 102249, China
[b] Xinjiang Oilfield Company Research Institute of Exploration & Exploitation, Karamay, Xinjiang, 834000, China
[c] CNOOC China Limited, Shenzhen Branch, Shenzhen, Guangdong, 518064, China

ARTICLE INFO

ABSTRACT

The determination of high-quality intervals in oil reservoirs has always been challenging work while their petrophysical attributes are relatively low. To date, extensive reservoir evaluation studies have been undertaken to locate favorable zones for oil exploration and exploitation. However, without the geological constraint principles, the selected evaluation parameters depend heavily on experience or pure mathematical methods. Hence, we propose a reservoir evaluation method based on petrophysical facies to undertake the reservoir quality assessment for the conglomerate reservoirs of the Triassic Baikouquan Formation in the northern Mahu sag, Junggar Basin, western China. The lithofacies and diagenetic facies were first identified based on laboratory data. Subsequently, petrophysical facies types were recognized by the combination of lithofacies and diagenetic facies. Afterward, capillary pressure curves of different petrophysical facies were clustered to clarify the reservoir quality variation in distinct geological origins. Consequently, the evaluation standard was established and the reservoir quality distribution was analyzed and drawn out. These results indicate that there exist 4 rock types in the Baikouquan Formation (from RT1 to RT4). The distributional status of the optimal reservoir (RT1) and the worst reservoir (RT4) are primarily determined by grain size, while rock type 2 (RT2) and rock type 3 (RT3) are predominantly controlled by dissolution and compaction. Moreover, an evident positive association exists between the rock type and the single well production capacity, which reveals that the utilization of petrophysical facies to assess reservoir quality is reliable. It is concluded that reservoir evaluation based on petrophysical facies harbors the potential to be a pivotal tool for reservoir property assessment and prediction of favorable porosity and permeability zones.

1. Introduction

Stimulated by the remarkable achievement of shale gas in North America, the untraditional hydrocarbon exploration in the People's Republic of China (PRC) has witnessed a major breakthrough (Yang et al., 2021; Li et al., 2021; Guo, 2021). Concurrently, the exploration and exploitation of low permeability oil resources have attracted great attention because of their industry-wise and commercial value. China's low permeability oil has huge exploration and development potential. By the end of 2018, the geological resources and technically recoverable resources stood at 178.2×10^8t and 12.34×10^8t, respectively (Gao and Yi, 2021). The low permeability oil reservoir in the PRC are widely distributed throughout major basins in China (Li et al., 2021; Zou et al., 2021) . The reservoirs are characterized by firm inhomogeneity and strong diagenesis. Therefore, the determination of high-quality zones in these reservoirs has turned into one of the most pivotal problems which have to be tackled.

To date, a lot of approaches have been proposed by researchers to determine the favorable zones (Hawkins, 2012; Li et al., 2021; Waqar and Murray, 2021; Fu et al., 2022; Su et al., 2021). The evaluation methods are transformed from traditional qualitative analysis to quantitative analysis. Concurrently, machine learning has been widely
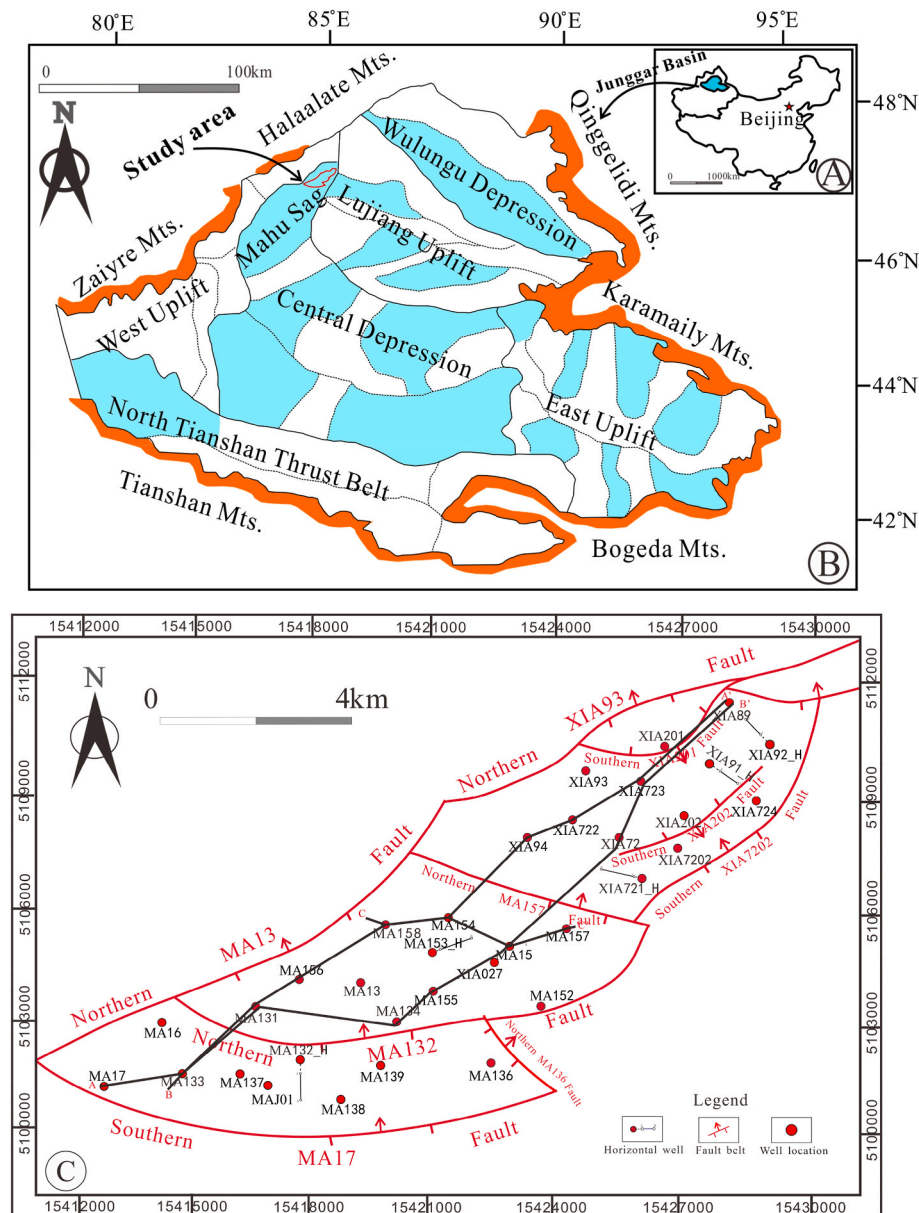
Fig. 1. (A) The map showing where Junggar Basin locates. (B) The structural map showing the location of the Mahu Sag and major tectonic units of Junggar Basin. The red polygon represents the study region. (C) The well location map of MA131 well block, the cross section in Figs. 3, 8 and 9 (outlined by the black line) and secondary thrust faults are also shown. (For interpretation of the references to color in this figure legend, the reader is referred to the Web version of this article.)

applied in reservoir evaluation, such as lithology, fluid, and fracture identification (Yu and Wang, 2021; Muhammad and Fang, 2021; Shu Su et al., 2022), parameter prediction (Mehdi and Aydin, 2021; Zhang et al., 2021; Pan and Zheng, 2021; Xue et al., 2022; Obed et al., 2021), as well as feature selection (Daniel and Tarek, 2021). Nevertheless, they are generally "black box" models, which brings extensive difficulties to explain. Various data and numerous factors are taken into consideration comprehensively, thus making the evaluation results increasingly accurate and precise (Wu et al., 2019; Xie et al., 2022; Zhang et al., 2021; Olmo et al., 2021; Su et al., 2021). Additionally, some special logging techniques are broadly employed to precisely undertake reservoir characterization work (Xu et al., 2019; Li et al., 2021; Thais et al., 2021; Li et al., 2021; Fan et al., 2021). The current research on reservoir evaluation has primarily concentrated on the selection of petrophysical parameters which depends heavily on research experience or pure mathematical methods without geological constraint principles. However, these parameters vary greatly in different target areas thereby

throwing obstacles for universal applicable reservoir quality assessment.

Junggar Basin is listed among China's large oleiferous basins, where tremendous hydrocarbon resources from the Triassic fan-delta conglomerate reservoirs are well-recorded (Wang et al., 2021). As one of the most vital regions for oil-gas exploration within the basin, the northwest Junggar Basin harbors 3.34×10^9t oil reserves, of which 1.34×10^9t are proven reserves, and 448×10^9 m^3 of gas reserves, of which 25.54×10^9 m^3 are proven reserves (Lei and Li, 2021). The latest discovery of the super-giant (over 1×10^9t of oil reserves) Mahu oilfield in the Triassic Baikouquan Formation unveils the remarkable oil potential of northwest Junggar Basin. Despite the significant hydrocarbon present, it is still challenging to locate areas with high porosity and permeability in the conglomerate reservoirs due to their low petrophysical properties. Greatly impacted by sedimentary environment, diagenesis, and tectonic movement, the target layer is featured by low porosity and ultralow permeability characteristics, and remarkable inhomogeneity. Previous studies predominantly utilize traditional
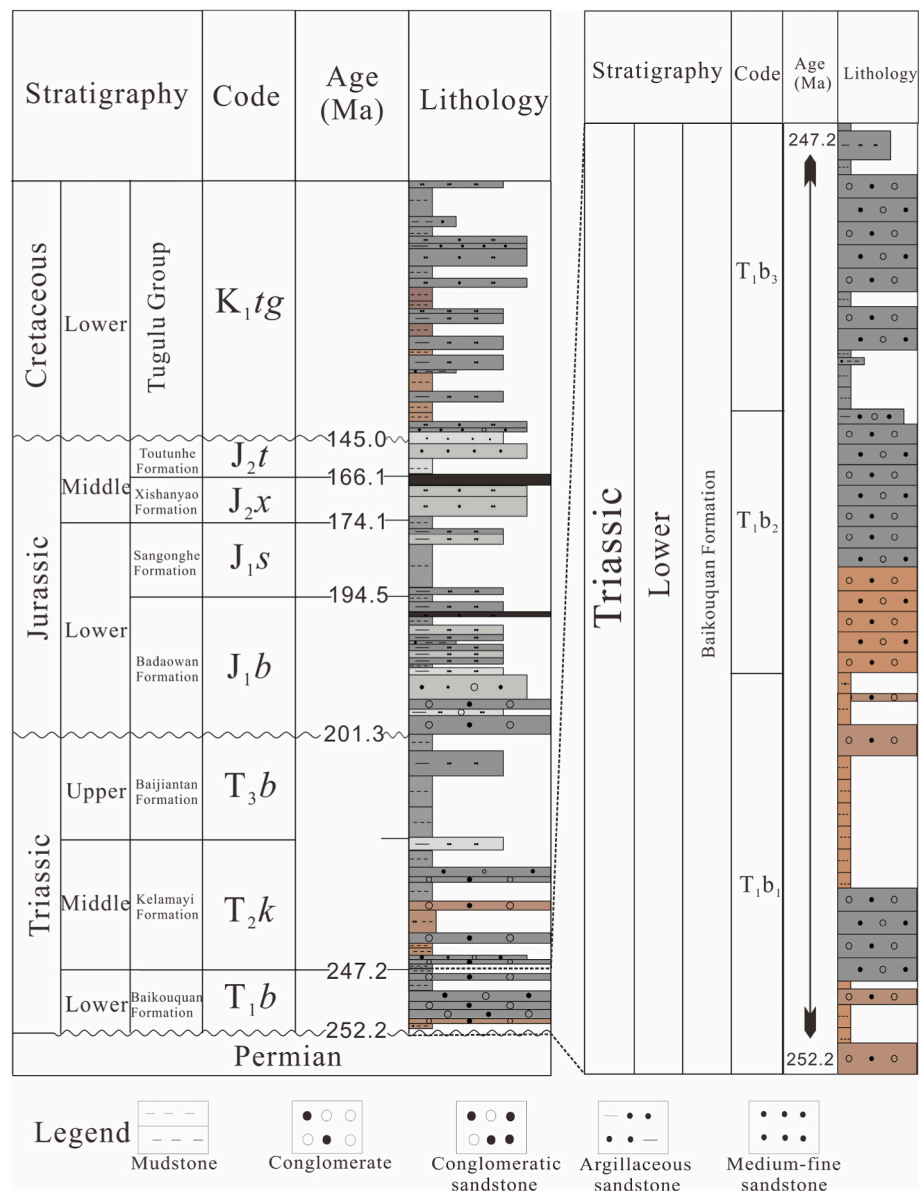
Fig. 2. Synthetical stratigraphic histogram of the strata in the research region. A high resolution sequence of the target layer is also shown on the right (modified from Xinjiang Oilfield).

evaluation methods to determine highly productive areas, such as parameter clustering, empirical statistical method, and oil-bearing condition (Lei and Li, 2021). However, these methods usually contradicted post-fracturing productivity. An evaluation method considering geological constraint principles is strongly demanded to throw light on subsequent advancement of oil exploration and exploitation.

To address the above problems, the concept of petrophysical facies is adopted for reservoir classification and evaluation. The definition originally emanated from Xiong and Peng (1994). It is defined as a reservoir genetic unit formed by various geological processes, which is a comprehensive effect of sedimentation, diagenesis, and later tectonic movement (Xiong and Wang, 2010). Petrophysical facies has the benefit of reflecting both the macro and micro petrophysical properties of the reservoir, as well as revealing the geological genetic mechanism of distinct petrophysical characteristics. Herein, a detailed examination is conducted by combining massive core descriptions, casting thin sections, scanning electron microscope (SEM) photos, together with capillary pressure curves to (1) determine the lithofacies and diagenetic facies of conglomerate reservoirs in this research; (2) categorize the rock

type and establish the evaluation standard by applying petrophysical facies; (3) explicate the controlling factors of the variation in reservoir quality and validate the effectiveness of the proposed method.

2. Geological settings

Junggar Basin is situated in north Xinjiang Province in northwest PRC (Fig. 1A). It has a total area of approximately 13×10^4 km^2 and is encircled by Paleozoic mountains, including northwestern Hala'alat and Zhayier, northeastern Kelameili, southeastern Bogeda, in addition, southwestern Yilinheibiergen (Fig. 1B). Mahu Sag, located on a pre-Carboniferous fold basement, is in Central Depression's northwest side of Junggar Basin. The shaping is greatly affected by its surrounding thrust activities. The Mahu Sag is delimited by eastern Dabasong and Xiayan uplifts and the western Kebai and Wuxia fault zones, as presented in Fig. 1B. The sag covers an area of 5000 km^2 and measures 100 km long and 50 km wide. Mahu Sag has undergone 3 primary tectonic activities dating from Late Carboniferous to Quaternary. The sag experienced large-scale tectonic action during the Late Permian epoch, and the
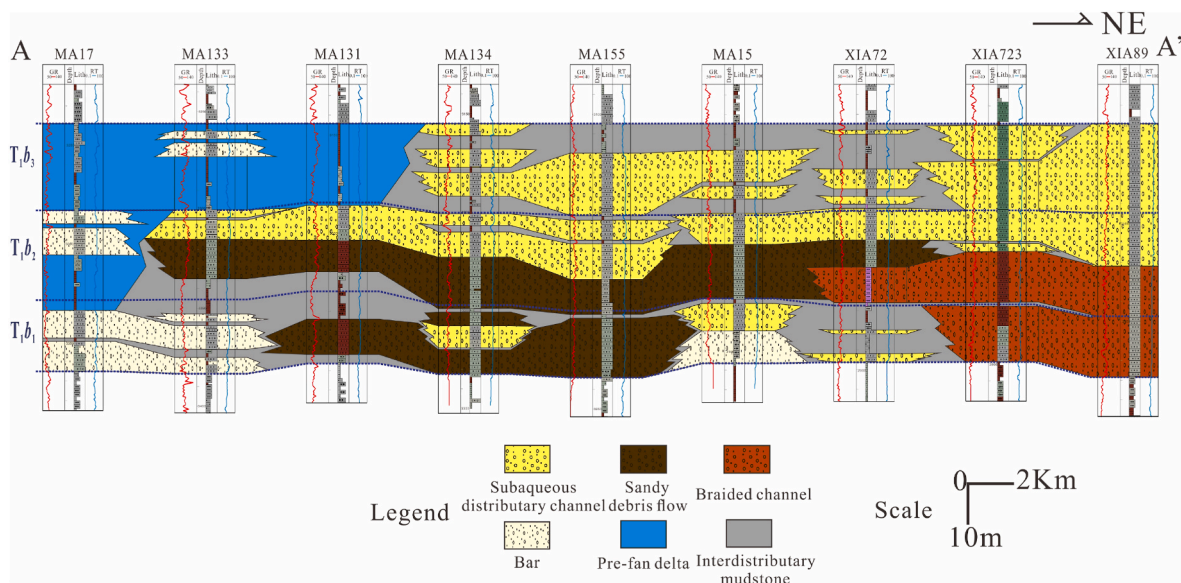
Fig. 3. Cross section parallel to the provenance direction showing the retrogradation of the fan delta complex in the research region. The location of the section can be seen in Fig. 1C.

foreland basin progressively transformed into a depression basin (Shan et al., 2016; Lu et al., 2019). Later tectonic activity appears to have slowed, and the strata have deposited intermittently, forming the current stratigraphical distribution pattern. The study focus, MA131 well block, is seated on the clival area of the northern Mahu Sag (Fig. 1C) and is predominated by the Xiazijie fan-delta sedimentary system. This region is a monocline inclining to the south with relatively gentle strata conditions. The sedimentary facies of Pre-fan delta, fan-delta front, and fan-delta plain had evolved from south to north in a successive way.

Within the study area, oil-gas reservoirs have been detected in Permian and Triassic strata, and oil yield from Triassic reservoirs takes up masses of overall oil yield. During the Triassic period, the strata of the Mahu Sag are composed of the lower Baikouquan, middle Karamay, and upper Baijiantan Formations (Tang et al., 2017). The Baikouquan Formation lies with an angular unconformity upon the underlying lower Wuerhe Formation (P_2w) of the Middle Permian and a conformable contact with the overlying Karamay Formation (T_2k) of the Middle Triassic. The Baikouquan Formation has a thickness ranging from 210 to 270 m. From bottom to top, the Baikouquan Formation is subdivided into 3 fourth-order sequences: T_1b_1, T_1b_2, and T_1b_3 (Yu et al., 2022) (Fig. 2). The lithology of T_1b_1 mainly comprises grayish brown conglomerates, exhibiting bell-shaped gamma-ray (GR). The lithology of sand group 1 of T_1b_2 is primarily gray conglomerate, whereas sand group 2 of T_1b_2 is mainly green–gray matrix-supported conglomerate. The lithology of T_1b_3 predominantly comprises gray conglomerates with thin sandstones and displays the characteristic of coarsening upward. This study mainly focuses on the T_1b_2 and T_1b_3, which is the primary pay zone of the Baikouquan Formation. From T_1b_1 to T_1b_3, the retrograded fan deltaic depositional system came into being in the process of lake transgression. The fan-delta front facies exist widely in the whole region (Fig. 3). In general, the fan-delta front in the research region comprises underwater distributary channels, mouth bars, and sandy debris flow. Many sets of thick glutenite developed successively, which create beneficial conditions for the forming of large-scale high quality lithologic reservoirs in the Baikouquan Formation of the Mahu sag (Yu et al., 2022).

3. Materials and methodology

Up till now, an overall 38 wells have been drilled into the Triassic strata, involving 34 vertical wells, and 4 horizontal ones, with most well

depths over 3000 m. A total of 212 thin sections, 306 SEM photos, 260 core petrophysical attribute data, and 178 capillary pressure curves from thirteen wells were acquired for analysis of the reservoir characteristics. Additionally, oil test and production data were also obtained from the Xinjiang oilfield company. Core samples (including thin sections) could provide the most direct evidence of lithology identification. Petrologic research could be completed via the analysis of thin sections and scanning electron microscope (SEM) photos, which are employed to analyze diagenesis as well. Moreover, conventional logging data, which are calibrated by cores and thin sections, could be sufficient information to construct logging interpretation models for the determination of lithofacies and diagenetic facies. The method flow is as follows:

(1) The lithofacies were determined through detailed and thorough core observation. After calibration by cores, logging responses of different lithofacies were then investigated to establish logging interpretation models for lithofacies identification in the Baikouquan Formation.

(2) Diagenesis analysis was carried out on account of thin sections and SEM photos. The diagenetic stage and diagenetic facies were then determined according to their characteristics under microscope. Through the above process, the electrical standard was also used to determine the diagenetic facies.

(3) The petrophysical facies type was defined via the combination of lithofacies and diagenetic facies. Next, the clustering of mercury injection capillary pressure parameters with these different petrophysical facies was performed to distinguish their reservoir quality variation.

(4) Eventually, we used the established reservoir evaluation standard based on petrophysical facies to categorize the rock type of every single well. The reservoir quality distribution maps were then drawn for the main development layers. Furthermore, production test data obtained from 34 wells in the Baikouquan Formation was employed for validation of the proposed method.

4. Results

4.1. Characteristics of reservoirs in the fan-delta complex

4.1.1. Lithofacies and their characteristics

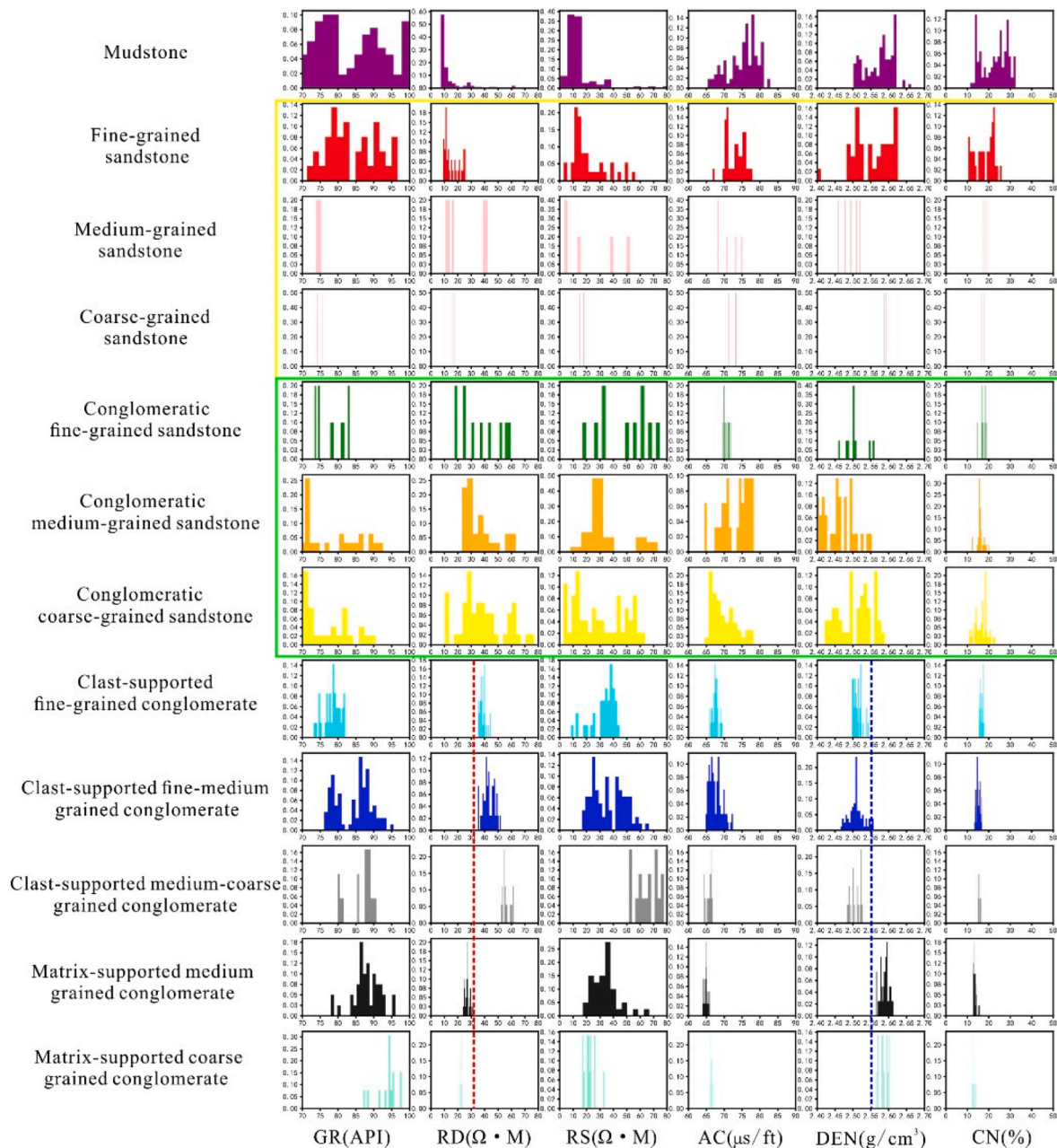Through detailed core observation, the lithofacies in the Baikouquan

Fig. 4. Conventional well logging characteristics of distinct lithofacies in the study interval.

Formation are complex and predominately consist of three lithological types: conglomerate, sandstone, and mudstone. Based on the grain size and clay content, a total of twelve lithofacies were identified. Calibrated by the cores and thin sections, their logging responses were investigated. As detailed in Fig. 4, different grain sizes of sandstone (seen in the yellow rectangle) and conglomeratic sandstone (seen in the green rectangle) are hard to differentiate due to their little logging response variation. Meanwhile, the matrix-supported conglomerate and clast-supported conglomerate are characterized by distinct resistivity and density values (seen in the red and blue dotted lines). Moreover, the gamma-ray and resistivity increased as the grain size became wider. As a result, the lithofacies in the Baikouquan Formation could be separated into eight sub-groups by well logs.

Matrix-supported conglomerates and clast-supported conglomerates dominate the target layer, accounting for ~90% of the lithofacies. The former is featured by poorly sorted and substantial high clay content. The gravels are suspended in the muddy matrix. In general, they are featured by stacked massive beddings originating from debris flow. Cores from depths of 3056.91 m and 3050.32 m in well MA154 of the Baikouquan Formation represent typical matrix-supported conglomerate samples with medium (with grain size>8 mm) and coarse grain size (with grain size>16 mm). The core specimen is gray in color and the gravel is dominated by volcanic rock debris (Fig. 5A and B). The conventional logging is featured by high natural gamma-ray radiation (>85API), low acoustics slowness, high density, low lateral resistivity, and medium-to-low compensated neutron log values. The clast-supported conglomerate core samples with different grain sizes were obtained at depth of 3095.17 m in Well MA15, 3048.02 m in well MA154, and 3302.66 m in well MA133 (Fig. 5C–E). They are poorly to moderately sorted and psephicity is commonly sub-rounded to sub-angular shapes, representing tractive current deposits evolved mainly in underwater distributary channels. Additionally, oil spots were identified in the course of the core sample studies as well (Fig. 5E). In contrast to matrix-supported conglomerates, which have comparatively
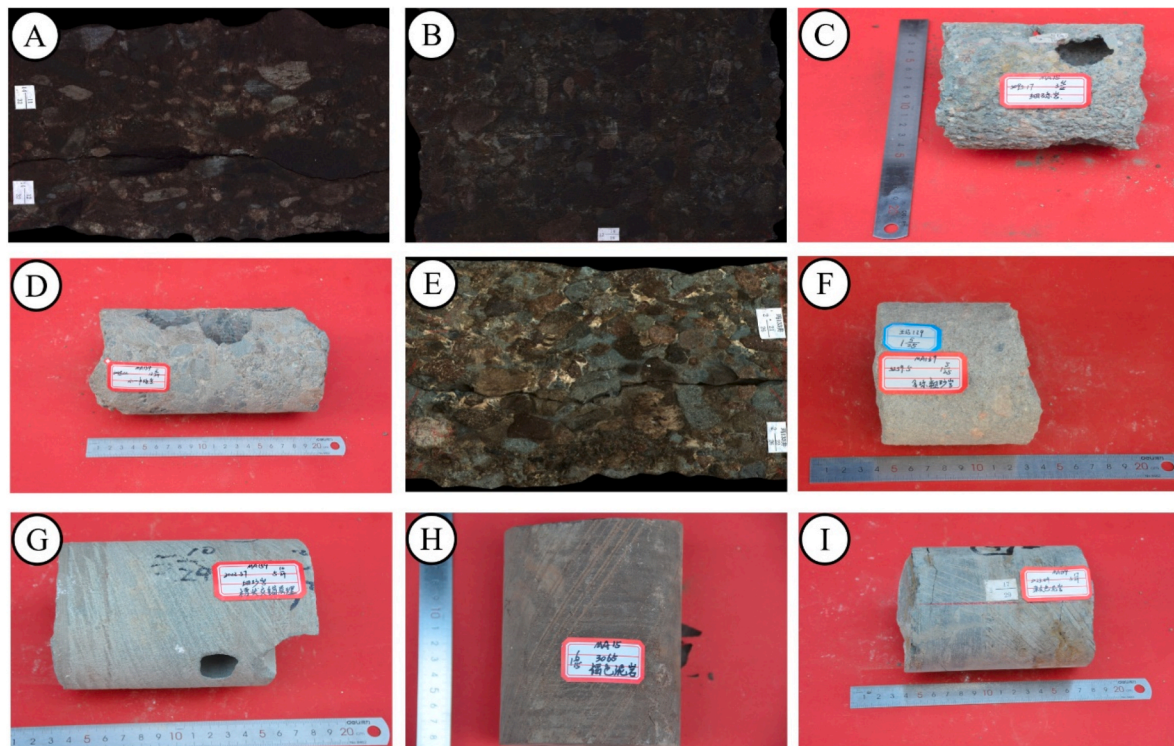
Fig. 5. Characteristics of conglomerate-dominated reservoir cores: (A) Matrix-supported medium grained conglomerates, bedding fracture was encountered, well MA154, 3056.91 m. (B) Matrix-supported coarse grained conglomerates, with grain size larger than 8 mm, well MA154, 3050.32 m. (C) Clast-supported fine-grained conglomerate, with grain size finer than 8 mm, moderate sorted, well MA15, 3095.17 m. (D) Clast-supported fine-medium grained conglomerate, poor sorted and sub-rounded, well MA154, 3048.02 m. (E) Clast-supported medium-coarse grained conglomerate, characterized by bedding fracture and oil spot could be observed, with grain size coarser than 16 mm, well MA133, 3302.66 m. (F) Conglomeratic coarse sandstone, with approximately 7% contents of conglomerates that can be observed, well MA139, 3259.50 m (G) Fine-medium grained sandstone, featured by trough cross-beddings, well MA154, 3022.37 m. (H) Brown mudstone, represents interdistributary fine-grained fillings, well MA15, 3065.00 m. (I) Dark-gray mudstone, with no obvious development of sedimentary structure, well MA154, 3023.49 m. (For interpretation of the references to color in this figure legend, the reader is referred to the Web version of this article.)
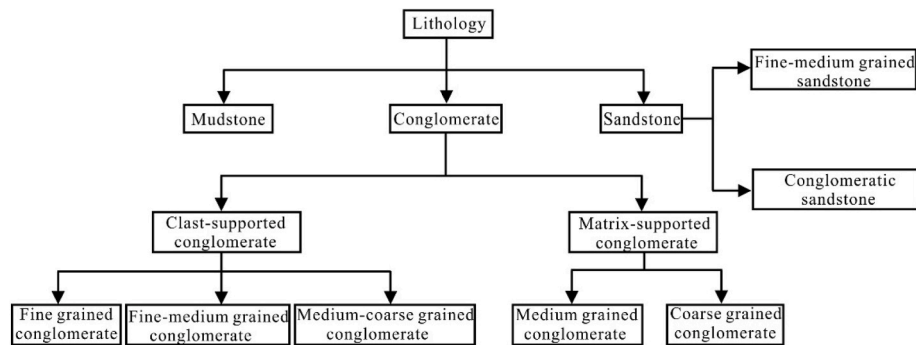

Fig. 6. Hierarchical framework of lithofacies identification in the study area.

higher density, the clast-supported conglomerates exhibit higher lateral resistivity, and lower density values. According to the grain size, it can be further divided into three subtypes: fine-grained conglomerate (with grain size<8 mm), fine-medium grained conglomerate (with grain size<16 mm), medium-coarse grained conglomerate (with grain size>16 mm). With the increase of granule size, the resistivity and gamma-ray values increase, while the density decreases.

The sandstones weren't well developed and primarily occurred in the distal of the fan-delta complex. The fine-medium sandstone owns excellent reservoir quality and is featured by trough cross-bedding (Fig. 5G). Such lithofacies reflects tractive current deposits evolved in subaqueous channels. The massive conglomeratic sandstone is light gray in color, with approximately 7% contents of conglomerates that can be observed (Fig. 5F). In general, the sandstone lithofacies are featured by

low density(<2.55 g/cm^3) and low resistivity values (<30 Ω M).

The mudstone is brown and gray, without evident development of depositional structure (Fig. 5H and I). Such lithofacies reflects interdistributary fine-grained fillings or pre-fan deltaic deposition corresponding to remarkably weak hydromechanics. The mudstone is featured by the highest density and lowest resistivity values.

Based on the rock physics analysis, a hierarchical framework of lithology identification is established in Fig. 6. Consequently, the corresponding interpretation chart is also drawn in Fig. 7.

4.1.2. Diagenetic characteristics

Although the reservoir in the Baikouquan Formation hasn't experienced potent tectogenesis, the conglomerate has undergone a long period of comparatively potent and intricate diagenetic evolution. The
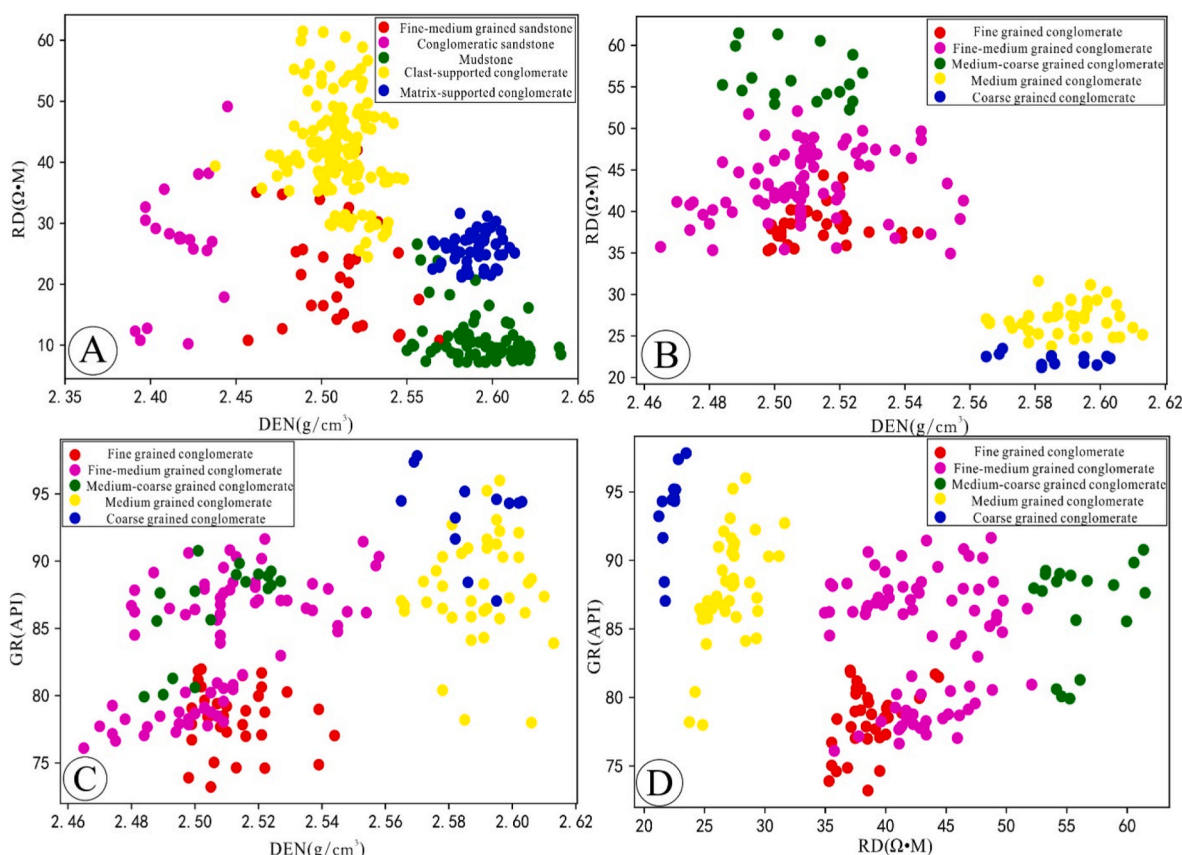
Fig. 7. Interpretation chart for lithofacies identification: (A) RD-DEN cross-plot to distinguish mudstone, sandstone, conglomerate; (B) RD-DEN cross-plot to distinguish conglomerate with different sedimentary mechanism; (C) GR-DEN cross-plot to distinguish conglomerate with different sedimentary mechanism; (D). GR-RD cross-plot to distinguish conglomerate with different sedimentary mechanism. RD refers to deep lateral resistivity; DEN refers to density; GR refers to gamma-ray.

main diagenetic types are presented in Fig. 8 and analyzed as follows.

4.1.2.1. Compaction. The primary cause of conglomerate compaction in the Baikouquan Formation is as follows (i): particulates exhibit plastic distortion (e.g. the rock debris is crooked, deformed, as detailed in Fig. 8A), and (ii): particulates display point-line connection and concave-convex connection (Fig. 8B). Generally, the quartz particulates demonstrate the greatest resistance to compaction, before feldspar. The thin section observation suggests strong compaction, resulting in a decrease in the aperture volume.

4.1.2.2. Cementation.

(1) Carbonate Cementation

Carbonate cement is the most common and frequently appears in the Baikouquan Formation. According to the internal XRD test data of Xinjiang Oilfield, its mass fraction ranges from 1% to 18%, with an average content of 6.45%. The most common carbonate cements are calcite and ferrous calcite, and their development often includes phases ≥1. Calcite is mostly featured by flake crystals filling the pores (Fig. 8D and E). Calcite cementation mainly occurred in the late diagenetic stage. A large amount of calcite began to appear in diagenetic authigenic minerals and then filled inter-granule apertures and dissolution apertures, resulting in the sharp exacerbation of reservoir attributes physically.

(2) Siliceous Cementation

The content of siliceous cement is low and developed unevenly

within the target layer. The high content of plastic rock debris is believed to have strengthened the compaction degree, causing the porosity to decrease rapidly, and there is not enough space for precipitation of autogenous siliceous cement. Cementation of siliceous minerals is merely formed in an acid condition. Siliceous precipitation happens once the level of silicon ions in the interstitial water surpasses the mean content, which mostly happens in the mesodiagenesis phase. As presented in Fig. 8F and G, the consequential autogenic siliceous cement predominantly consist of overgrowth rims along the edge of microcrystalline components or appear as euhedral prismatic shapes filling the pores. The occurrence of both quartz overgrowth and individual microcrystal causes remarkable pore-filling, a reduction of porosity, together with a smaller pore-throat radius and non-efficient permeation capability.

(3) Cementation of Clay Minerals

The research into clay materials is a pivotal part of diagenetic process, and determining and dividing diagenesis phases. The kinetics of diagenesis environment and fluid attributes makes it possible for diverse clay mineral categories to be apt to convert into one another. As detailed in Fig. 8H–J, the main constituents of the clay materials of the Baikouquan Formation are kaolinite, illite-smectite mixed-layer, together with chlorite. Illite-smectite mixed-layer appears in a honeycomb-like shape in the pore throat (Fig. 8H), which severely decreases the seepage capacity of the reservoir. During the eodiagenesis, kaolinite occurs in the intergranular pores in worm-shaped form (Fig. 8I). However, as the diagenetic environment is converted to an alkaline environment, kaolinite turns into chlorite under the existence of iron and magnesium ions. Previous studies have indicated that substantial iron ions, which
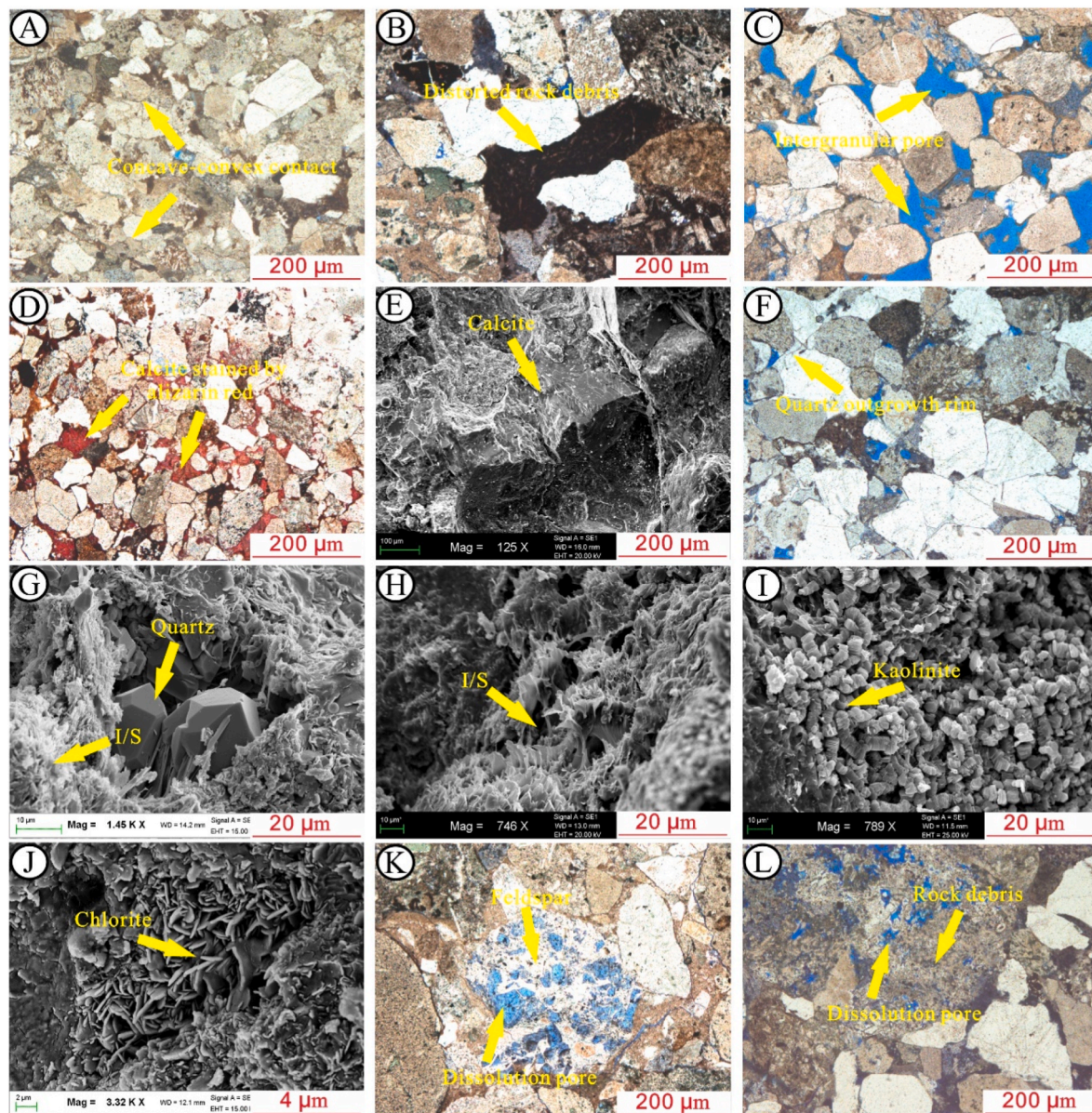
Fig. 8. Main diagenetic characteristics of conglomerate reservoirs in the Baikouquan Formation: (A) Detrital particles exhibit concave-convex contacts (well XIA723, 2700.36 m, XPL). (B) Rock debris bending deformation (well MA154, 3006.53 m, XPL). (C) Residual intergranular pores can be observed due to weak compaction (well MA139, 3258.11 m, XPL). (D) Crystalline calcite fills the intergranular pores, (well MA154, 3054.85 m, XPL). (E) Granulated crystal construction of calcite, (well MA13, 3107.29 m, SEM). (F) Quartz overgrowth can be observed, (well XIA89, 2477.27 m, XPL) (G) Autogenous quartz, attached to the I/S, fills the intergranular pores (well MA16, 3220.19 m, SEM). (H) Autogenous I/S fills the intergranular pores(well MA131, 3188.89 m, SEM). (I) Kaolinite occurs in the intergranular pores in a worm-shaped form (well MA132, 3261.37 m, SEM). (J) Leaf-shaped chlorite wraps the particle (well MA16, 3213.77 m, SEM). (K) Strong dissolution of feldspar particle (well MA154, 3051.83 m, XPL). (L) Dissolution of rock debris (well MA152, 3096.70 m, XPL).

mainly originated from the alteration of volcanic rock debris, are required to realize the formation of the chlorite coatings (Cao et al., 2018). Therefore, the growth of leaf-shaped chlorite begins to come into being around the margin of detrital particulates and eventually wraps the particulates completely in a chlorite membrane (Fig. 8J). It's broadly believed that such a chlorite membrane prevents the particulates from contacting the interstitial water, which has restrained the overgrowth of quartz. The resultant formation of chlorite casts a protection influence on the primary intergranular porosity through an effect of anti-compaction.

4.1.2.3. Dissolution. Dissolution is vital for enhancing the petrophysical attributes of the reservoir throughout the entire diagenetic process. In an acid surrounding, plastic rock debris and feldspar are easily dissolved

(Fig. 8K and L). The reservoir is predominated by the feldspar dissolution which occurs in the orientation of cleavage cracks, yielding an extra induced porosity. Apart from the residual intergranular apertures (Fig. 8C), the dissolution pores are vital for petroleum accumulation in the Baikouquan Formation.

In general, the diagenetic facies in the Baikouquan Formation were categorized mainly into five forms according to the above detailed observation: weak compaction facies, dissolution facies of unstable components, clay mineral-cementation facies, cementation facies of calcite, densification facies of compaction. After calibration with the conventional logging data, the electrical characteristics of these diagenetic facies were shown in Fig. 9. The well log response of calcite cementation is characterized by high resistivity (>60 Ω m) and low acoustic slowness values (<65 μs/ft). Clay mineral-cementation shows
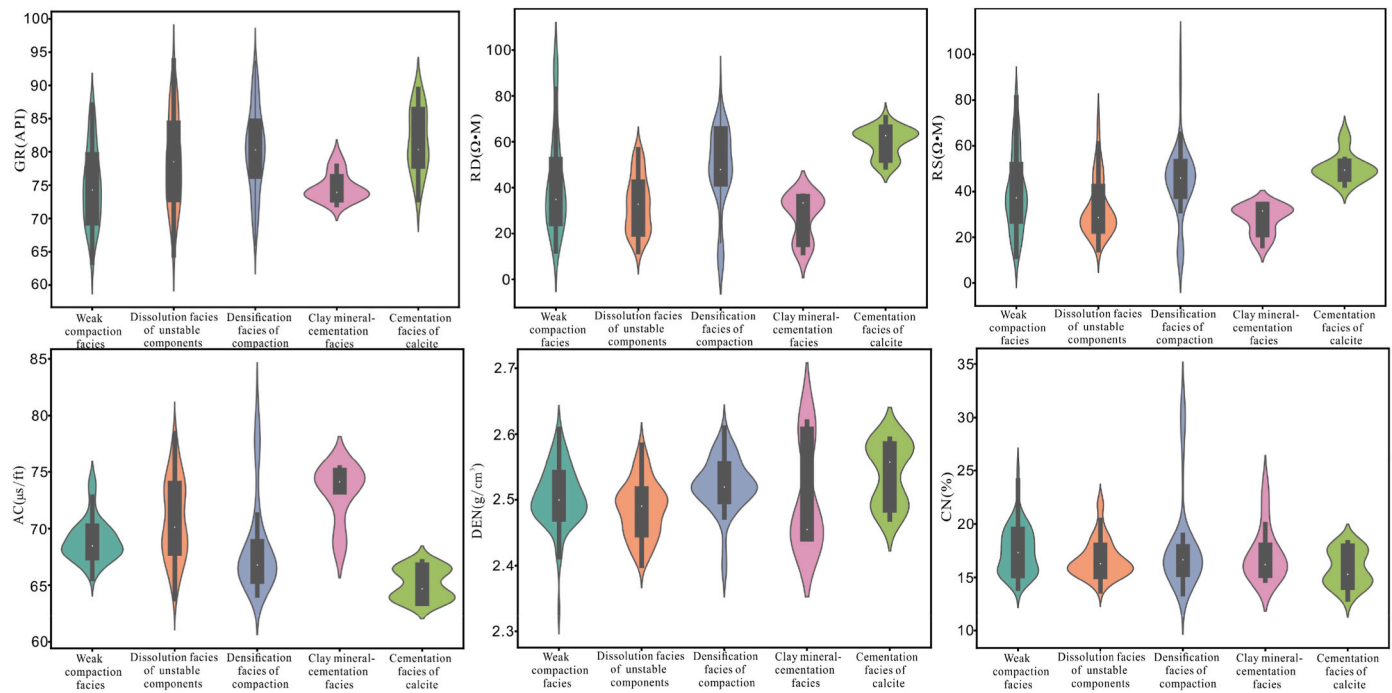
Fig. 9. Conventional well logging responses of diagenetic facies.

Table 1
Well log responses of different diagenetic facies.

Diagenetic facies	GR (API)	AC(us/ft)	RHOB(g/cm³)	CNL(%)	RD(Ω·M)	RS(Ω·M)
Weak compaction facies	65.4–85.8/72.8	65.0–73.3/67.8	2.46–2.66/2.49	13.1–23.0/17.2	12.1–65.6/34.6	13.1–68.8/38.4
Dissolution facies of unstable components	68.8–90.1/76.5	64.2–75.7/67.9	2.38–2.59/2.47	13.2–22.5/16.8	15.8–62.7/31.3	16.5–61.3/35.2
Densification facies of compaction	68.3–93.3/80.7	60.2–71.7/65.3	2.45–2.64/2.54	12.5–20.5/14.7	24.4–76.2/42.1	21.2–61.5/46.4
Cementation facies of clay minerals	70.7–84.5/74.2	66.3–77.8/73.6	2.41–2.64/2.51	12.6–24.4/16.0	15.9–42.5/34.6	14.4–42.5/31.6
Cementation facies of calcite	71.8–94.1/82.3	61.8–67.1/64.3	2.43–2.64/2.57	11.4–21.1/15.5	50.6–80.8/60.4	39.2–65.0/54.3
Minimum-Maximum/Average						

the highest acoustic slowness values (>74 µs/ft), whereas the other four types are lower than 70 µs/ft (Fig. 9). The densification facies of compaction is featured by relatively high density values (>2.55 g/cm³) and the two constructive diagenetic facies show lower density values (<2.5 g/cm³) (Table 1).

4.1.3. Pore-throat structure

According to the analysis of mercury injection parameters, the capillary pressure curve of the Baikouquan Formation reservoir is characterized by fine skewness, high displacement pressure and low mercury-ejection efficiency. Median pressure ranges from 4 MPa to 20.4 MPa, with a mean of 11.7 MPa. The median radius varies between 0.04 µm and 0.31 µm. The average displacement pressure and capillary radius are 0.54 MPa, and 0.52 µm, respectively. Overall, the pore structure is characterized by medium to low porosity, micro throat, and poor seepage capacity. Large-scale fracturing is the premise and effective approach to improve the seepage capacity and productivity for this kind of reservoir.

4.2. Petrophysical facies type and their reservoir quality variation

4.2.1. Petrophysical facies type

The petrophysical facies (PF) is a geological unit with alike sedimentary and diagenetic characteristics. According to the detailed observation in section 4, summing those identifications, 12 petrophysical facies types are identified by combining lithofacies and diagenetic facies in the Baikouquan Formation (Table 2).

PF1 (Fine-medium grained sandstone - Weak compaction facies): This lithofacies is fine-medium grained sandstone and the main diagenetic facies is weak compaction facies. The clastics are well sorted and are < 1 mm in diameter. The aperture types predominantly comprise intergranular apertures with comparatively good connection. The PF1 evolved in subaqueous distributary channels and mouth bars.
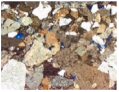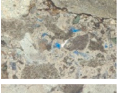
PF2 (Conglomeratic sandstone - Weak compaction facies): Such lithofacies is conglomeratic sandstone and the major diagenetic facies is weak compaction facies. The particles are well sorted and sub-rounded, with particle sizes smaller than 2 m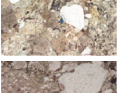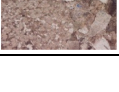m in diameter. The aperture types primarily comprise inter-granule apertures. The PF2 was developed in an alike geology setting as that of PF1.

PF3 (Fine grained conglomerate - Weak compaction facies): Such lithofacies is fine grained conglomerate whereas the diagenetic facies is primarily weak compaction facies. The rock particulates comprise well-sorted and rounded gravel, and the aperture type is predominantly intergranular aperture. The pores have good connectivity. The PF3 clearly appeared to have the characteristics of tractive current deposits and were mainly developed in subaqueous distributary channels.

PF4 (Fine grained conglomerate - Clay mineral-cementation facies): Such lithofacies is fine grained conglomerate and the diagenetic facies is mainly clay mineral-cementation facies. The petrophysical properties are poor due to the pore reduction caused by the precipitation of clay minerals, and the pore type is primarily micropore. The PF4 was mainly developed in subaqueous distributary channels.

PF5 (Fine-medium grained conglomerate - Dissolution facies of unstable components): This lithofacies is fine-medium grained

Table 2
Geological characteristics of geogenic petrophysical facies.

Petrophysical facies	Sedimentary microfacies	Lithofacies	Diagenetic facies	Pore type	Thin section
PF1	Subaqueous distributary channel; mouth bar	Fine-medium grained sandstone	Weak compaction facies	Intergranular pore	
PF2	Subaqueous distributary channel; mouth bar	Conglomeratic sandstone	Weak compaction facies	Intergranular pore	
PF3	Subaqueous distributary channel	Fine grained Conglomerate (Clast supported)	Weak compaction facies	Intergranular pore	
PF4	Subaqueous distributary channel	Fine grained Conglomerate (Clast supported)	Clay mineral- cementation facies	Micro pore; Intercrystalline pore	
PF5	Braided channel; Subaqueous distributary channel	Fine-medium grained conglomerate (Clast supported)	Dissolution facies of unstable components	Intragranular pore	
PF6	Braided channel; Subaqueous distributary channel	Fine-medium grained conglomerate (Clast supported)	Weak compaction facies	Intergranular pore	
PF7	Braided channel; Subaqueous distributary channel	Fine-medium grained conglomerate (Clast supported)	Densification facies of compaction	Micro pore	
PF8	Braided channel; Subaqueous distributary channel	Fine-medium grained conglomerate (Clast supported)	Cementation facies of calcite	Intergranular pore	
PF9	Braided channel;	Medium-coarse grained conglomerate (Clast supported)	Dissolution facies of unstable components	Intragranular pore	
PF10	Braided channel;	Medium-coarse grained conglomerate (Clast supported)	Weak compaction facies	Intergranular pore	
PF11	Sandy debris flow	Medium grained conglomerate (Matrix supported)	Densification facies of compaction	Micro pore	
PF12	Sandy debris flow	Coarse grained conglomerate (Matrix supported)	Densification facies of compaction	Micro pore	

conglomerate and the diagenetic facies is mainly dissolution facies of unstable components. The porosity increases resulting from the dissolution of unstable minerals like feldspar or rock debris, and its aperture type is mainly composed of secondary dissolution pores. The PF5 was mainly developed in subaqueous distributary channels and braided channels.

PF6 (Fine-medium grained conglomerate - Weak compaction facies): This lithofacies is fine-medium grained conglomerate and the diagenetic facies is predominantly weak compaction facies. The rock particulates comprise moderately-sorted and sub-rounded gravel, and the aperture type is predominantly intergranular aperture. The PF6 was mainly developed in subaqueous distributary channels and braided channels.

PF7 (Fine-medium grained conglomerate - Densification facies of compaction): This lithofacies is fine-medium grained conglomerate and the diagenetic facies is mainly densification facies of compaction. The particles are composed of poorly-sorted and sub-angular gravel and exhibit concave-convex contacts. The pore type is primarily micropore. The PF7 was mainly developed in subaqueous distributary channels.

PF8 (Fine-medium grained conglomerate - Cementation facies of

calcite): This lithofacies is fine-medium grained conglomerate and the diagenetic facies is mainly cementation facies of calcite. The particles are moderately sorted and sub-rounded, with particle sizes smaller than 8 mm in diameter. The pore type is primarily micropore. The PF8 was mainly developed in subaqueous distributary channels and braided channels.

PF9 (Medium-coarse grained conglomerate - Dissolution facies of unstable components): This lithofacies is fine-medium grained conglomerate and the diagenetic facies is mainly dissolution facies of unstable components. The particles are moderately sorted and sub-angular, with grain size larger than 8 mm in diameter. The pore type is primarily dissolution pore. The PF9 was mainly developed in braided channels.

PF10 (Medium-coarse grained conglomerate - Weak compaction facies): This lithofacies is fine-medium grained conglomerate and the diagenetic facies is mainly weak compaction facies. The particles are mainly composed of rigid gravel and show point-line contacts, with grain sizes larger than 8 mm in diameter. The pore type is primarily intergranular pore. The PF10 was mainly developed in the same
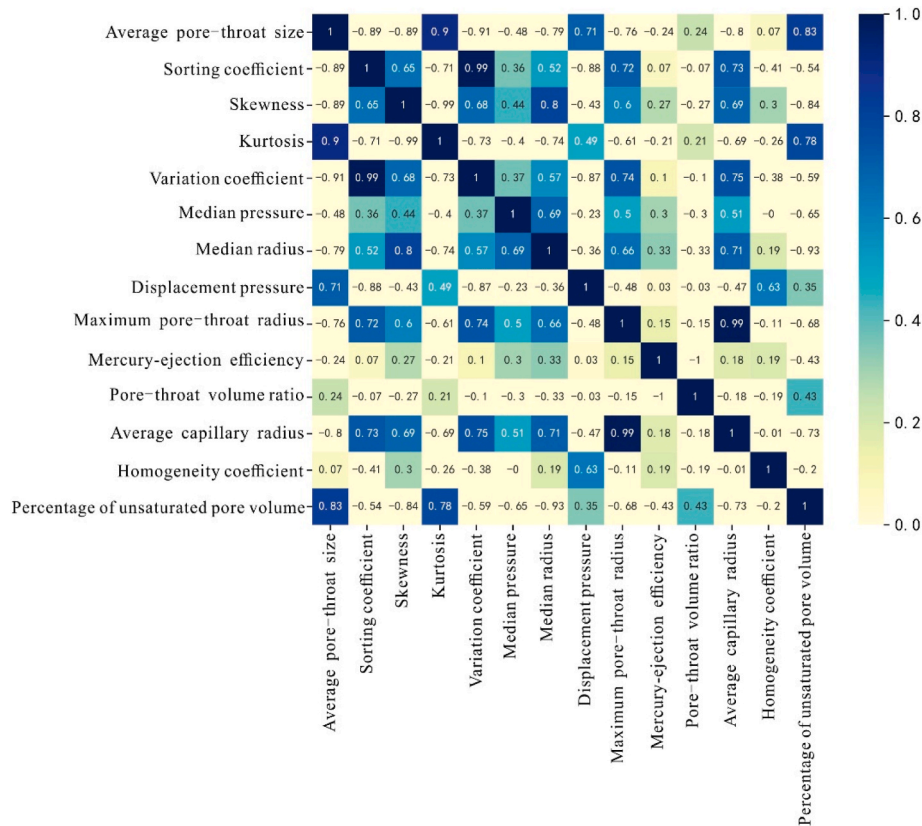
Fig. 10. Correlation coefficient matrix of each capillary pressure parameter.

geological setting as that of PF9.

PF11 (Matrix supported medium grained conglomerate - Densification facies of compaction): This lithofacies is matrix-supported medium grained conglomerate and the diagenetic facies is mainly densification facies of compaction. The particles are mainly suspended in the muddy matrix, with particle sizes smaller than 8 mm in diameter. The pore type is primarily micropore. The PF11 appeared to have the characteristics of gravity current deposits and were mainly developed in sandy debris flow.

PF12 (Matrix supported coarse grained conglomerate- Densification facies of compaction): This lithofacies is matrix-supported conglomerate with coarse grain size and the diagenetic facies is mainly densification facies of compaction. The particles are mainly suspended in the muddy matrix, with grain size larger than 8 mm in diameter. The pore type is primarily micropore. The PF12 was developed in the same environment as that of PF11.

4.2.2. Reservoir quality variation

After the petrophysical facies have been identified, their reservoir quality variation was investigated using capillary pressure parameters, which reveal the pore-throat structure and determine the mercury-injection curve morphological characteristics. A total of 178 capillary pressure curves were acquired from the oilfield. The capillary pressure parameter of each sample is regarded as a vector in p-dimensional space, $Xn = \{Xn\ (d),\ d = 1,2, \ldots, P\}$. The correlation coefficient P_{ij} between the i-th sample and the j-th sample can be derived from the following formula:

$$p_{ij} = \frac{E[(X - \mu x)(Y - \mu y)]}{\sigma_X \sigma_Y} = \frac{\sum\limits_{k=1}^{P} (x_{ik} - \mu x_i)(x_{jk} - \mu x_j)}{\sqrt{\sum\limits_{k=1}^{P} (x_{ik} - \mu x_i)^2} \sqrt{\sum\limits_{k=1}^{P} (x_{jk} - \mu x_j)^2}} \tag{1}$$

where X_i denotes the i-th sample, X_j denotes the j-th sample, X_{ik} denotes the k-th parameter in sample X_i. Afterward, the correlation coefficient matrix between capillary pressure parameters was calculated (Fig. 10). Subsequently, principal component analysis was performed for the purpose of reduction of unsuitable parameters, which greatly simplifies the clustering model. Eventually, the selected parameters were clustered using the k-means method to divide rock types.

Consequently, all rock types exhibit an alike set of capillary pressure curves and similar pore throat distribution characteristics (Fig. 11). The results indicate that each rock type shows a distinct capillary pressure curve set and pore throat radius distributional characteristics, which are remarkably diverse in reservoir quality. From the first to the fourth rock type, the median pressure is increasing, the average pore throat radius is decreasing in turn, revealing that the petrophysical properties are getting worse.

Four rock types were clustered from twelve petrophysical facies, which display remarkable diversity in reservoir property. The reservoir types consist of distinct geological genetic petrophysical facies and can be explained as follows:

Rock type 1 (RT1): this is composed of PF1, PF2, PF3 and PF5. RT1 belongs to the optimal reservoir property with great porosity and permeability (Fig. 12 A, B). It features the lowest displacement pressure and maximum mercury saturation. The lithofacies are fine-medium grained sandstone, conglomeratic sandstone, fine and fine-medium grained conglomerate. The major diagenetic type is weak compaction. The aperture types are predominantly intergranular and intragranular pores with good connection among the apertures.

Rock type 2 (RT2): this consists of PF6, PF9, and PF10 (Fig. 12 C, D). RT2 is of medium-high reservoir quality. It is characterized by low-medium displacement pressure and with an average of 60% mercury saturation. The lithofacies are fine-medium and medium-coarse grained conglomerates. The major diagenetic type is weak compaction and dissolution of unstable components. The aperture types are
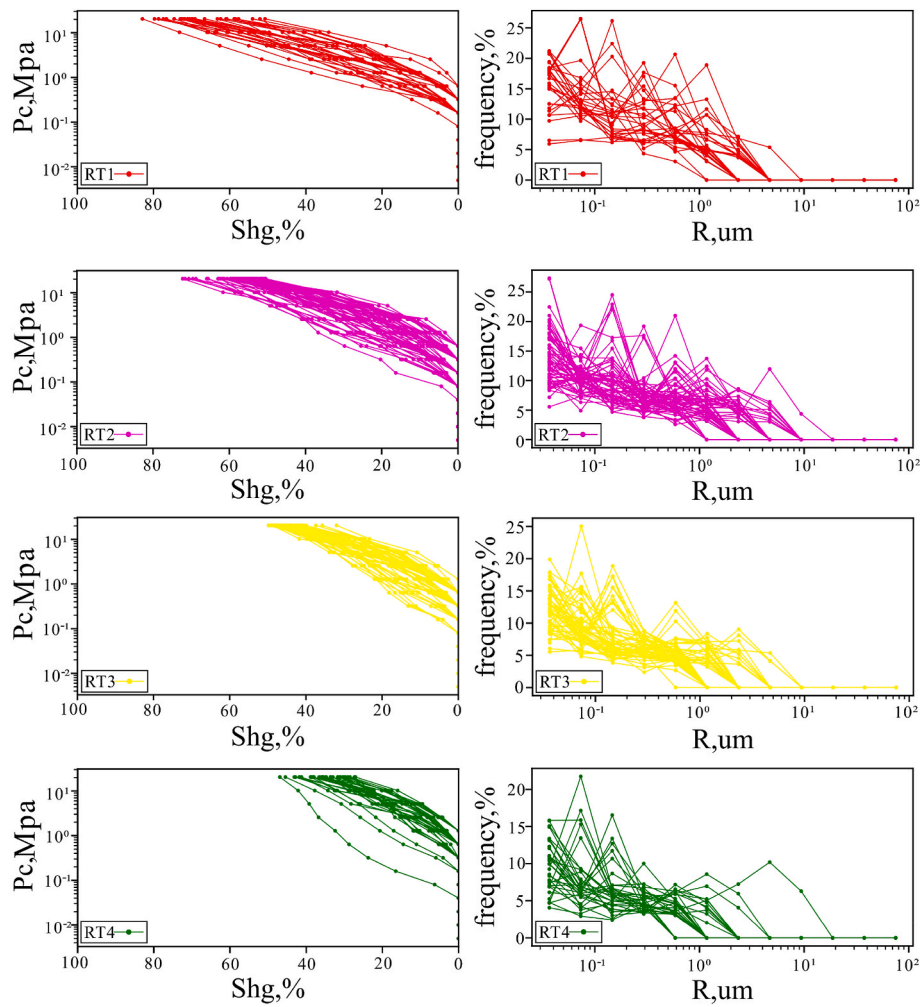
Fig. 11. Mercury injection curves and pore-throat radius of different rock types. From RT1 to RT4, the mercury saturation and pore-throat radius are decreasing. Pc denotes capillary pressure; Shg denotes mercury saturation; R denotes pore throat radius.

predominantly intragranular and intergranular pores with relatively poor connectivity.

Rock type 3 (RT3): this constitutes PF4 and PF7 (Fig. 12 E, F). RT3 is of low-medium reservoir quality. It is featured by high displacement pressure with mercury replete degree lower than 50%. The lithofacies are fine and fine-medium grained conglomerates. The main diagenetic type is cementation of clay minerals and strong compaction. The pore types are predominantly intercrystalline pores and micropores with pretty poor connectivity.

Rock type 4 (RT4): this is made up of PF8, PF11 and PF12 (Fig. 12 G, H). RT4 has the worst reservoir quality. It is featured by the highest displacement pressure with a mercury saturation of 40%. The lithofacies are fine-medium grained conglomerates, matrix-supported medium grained (with grain size>8 mm) and coarse grained (with grain size>16 mm) conglomerates. The main diagenetic types are strong compaction and cementation of calcite. The pore types are predominantly micropores.

4.3. Establishment of evaluation standard

To determine the pore-throat radius Ri (relevant pore throat diameter when the mercury saturation is i%) which reflects the seepage capacity, we developed a series of empirical formulas between porosity, permeability, and the computation of pore-throat radius in correspondence to mercury replete degree between 5% and 60% by increments of five (Table 3).

It comes out in Table 3 that the change of correlation coefficient shows a trend of increasing first and then decreasing. When I% is 15%, the correlation coefficient is the highest. The results show that for the low permeability conglomerate reservoir, when the mercury saturation hits 15%, the mercury will form a comparatively successive permeation channel within the rock. When such saturation is below 15%, the successive permeation channel won't form. Although the corresponding pore throat radius is relatively large, its contributing effects to the whole seepage capacity are restricted. In contrast to conventional reservoirs, the best mercury saturation value (15%) of the low permeability conglomerate reservoirs in the Baikouquan Formation is smaller.

It can be concluded that R_{15} is the key parameter determining the pore structure characteristic and seepage capacity. Although there exist numerous factors that affect the pore-throat structure of the reservoir, for instance, the diversity of grain size, sorting differentiation caused by sedimentation, and the diversity of diagenetic types, i.e., the degree of compaction, cementation, and dissolution. These factors ultimately reflect the variation in reservoir quality. As shown in Fig. 13, the rock type based on petrophysical facies could also be divided by certain R_{15} values, which verified the rationality employing the petrophysical facies to undertake reservoir evaluation work. Through the above comprehensive research, a newly conglomerate reservoir evaluation standard that reflects the main controlling factors of reservoir quality is established in Table 4.
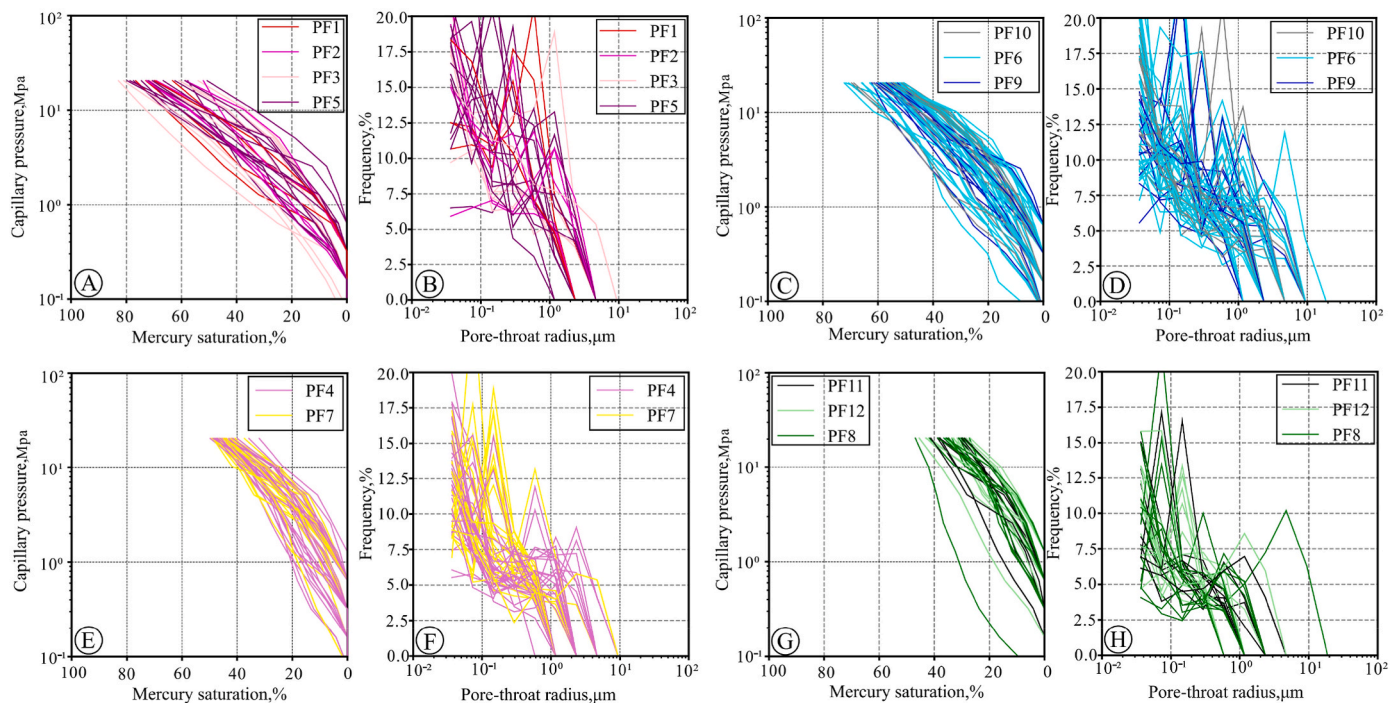
Fig. 12. The clustering analyses of geological genetic petrophysical facies in different rock types.

Table 3

Empirical equations for determining optimal seepage pore-throat radius. K_{air} denotes air permeability, mD; φ_{core} denotes measured core porosity, fraction.

No	Equations	Correlation coefficient
1	$Log(r_5) = -0.389 \log(K_{air}) + 1.539 \log(\varphi_{core}) - 1.219$	0.745
2	$Log(r_{10}) = -0.355 \log(K_{air}) + 1.416 \log(\varphi_{core}) - 1.276$	0.792
3	$Log(r_{15}) = -0.408 \log(K_{air}) + 1.472 \log(\varphi_{core}) - 1.460$	0.796
4	$Log(r_{20}) = -0.304 \log(K_{air}) + 1.570 \log(\varphi_{core}) - 1.707$	0.739
5	$Log(r_{25}) = -0.354 \log(K_{air}) + 1.397 \log(\varphi_{core}) - 1.674$	0.659
6	$Log(r_{30}) = -0.236 \log(K_{air}) + 1.631 \log(\varphi_{core}) - 2.037$	0.653
7	$Log(r_{35}) = -0.136 \log(K_{air}) + 1.521 \log(\varphi_{core}) - 2.083$	0.636
8	$Log(r_{40}) = -0.084 \log(K_{air}) + 1.788 \log(\varphi_{core}) - 2.435$	0.698
9	$Log(r_{45}) = -0.054 \log(K_{air}) + 1.877 \log(\varphi_{core}) - 2.619$	0.755
10	$Log(r_{50}) = 0.177 \log(K_{air}) + 1.920 \log(\varphi_{core}) - 2.790$	0.763
11	$Log(r_{55}) = 0.153 \log(K_{air}) + 1.866 \log(\varphi_{core}) - 2.882$	0.779
12	$Log(r_{60}) = 0.173 \log(K_{air}) + 1.956 \log(\varphi_{core}) - 3.098$	0.771

4.4. Distribution of reservoir quality

Following the establishment of the reservoir evaluation standard and the well log responses of lithofacies and diagenetic facies, the rock type of all single wells in the Baikouquan Formation are interpreted. Accordingly, several cross sections parallel and perpendicular to the provenance direction are selected to validate the effectiveness of reservoir evaluation based on petrophysical facies. Consequently, the plane distribution maps of rock type of sand group 1 of T_1b_2 and T_1b_3 were drawn thereby locating high-quality reservoirs.

4.4.1. Vertical distribution of single well

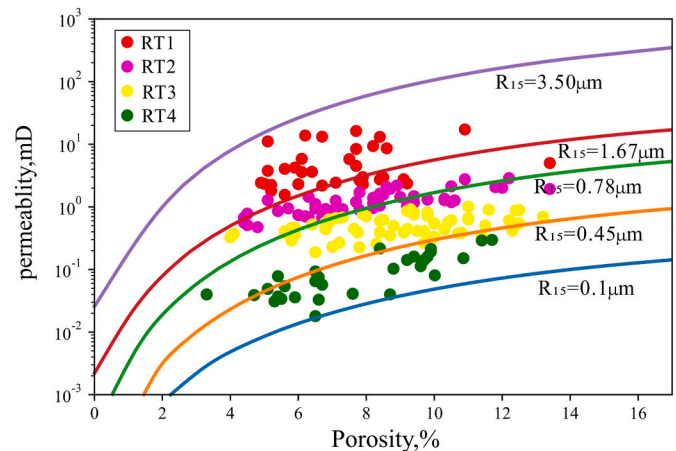For each single well, the rock type is identified by its lithofacies and

Fig. 13. The clustering analyses of geological genetic petrophysical facies in different rock types. The rock type based on petrophysical facies could also be divided by certain R_{15} values.

diagenetic facies. Diagenetic facies is basically controlled by lithofacies. Favorable diagenetic facies is always associated with lithofacies belt such as fine grained or medium grained conglomerates. Therefore, lithofacies is the basis for forming "sweet spot" of conglomerate reservoirs, and the reformation of diagenesis is the key to forming "sweet spot". The comprehensive action of lithofacies and diagenesis controls the pore structure, that is, the formation and distributional status of high quality reservoirs, which further determines the micro-scale hydrocarbon accumulation. It is concluded that the interval where RT1 and RT2 are developed can be interpreted as the "sweet spot" in the conglomerate reservoirs. Combined with oil test results, the oil reservoirs have an intimate association with high quality reservoirs (namely RT1, RT2). On the contrary, the oil test or logging interpretations which are mostly dry or poor oil reservoirs are consistent with RT3 or RT4. For instance, in the 3048–3056 m depth interval of well MA15 where RT1 is encountered (Fig. 14), the oil test (3 mm nozzle, 17.2Mpa flowing tubing pressure)

Table 4

Reservoir evaluation standard in theBaikouquan Formation.

Rock type	Petrophysical facies	R_{15} (µm)	Macroporosity (%)	Permeability (mD)	Pore type
RT1	PF1	>1.67	>8	1.1–10	Intergranular pore; Intragranular pore
	PF2				
	PF3				
	PF5				
RT2	PF6	0.78–1.67	8–10	0.4–1.1	Intergranular pore; Intragranular pore
	PF9				
	PF10				
RT3	PF4	0.45–0.78	6–10	0.1–0.4	Micro pore; Intercrystalline pore
	PF7				
RT4	PF8	0.1–0.45	<6	<0.1	Micro pore
	PF11				
	PF12				
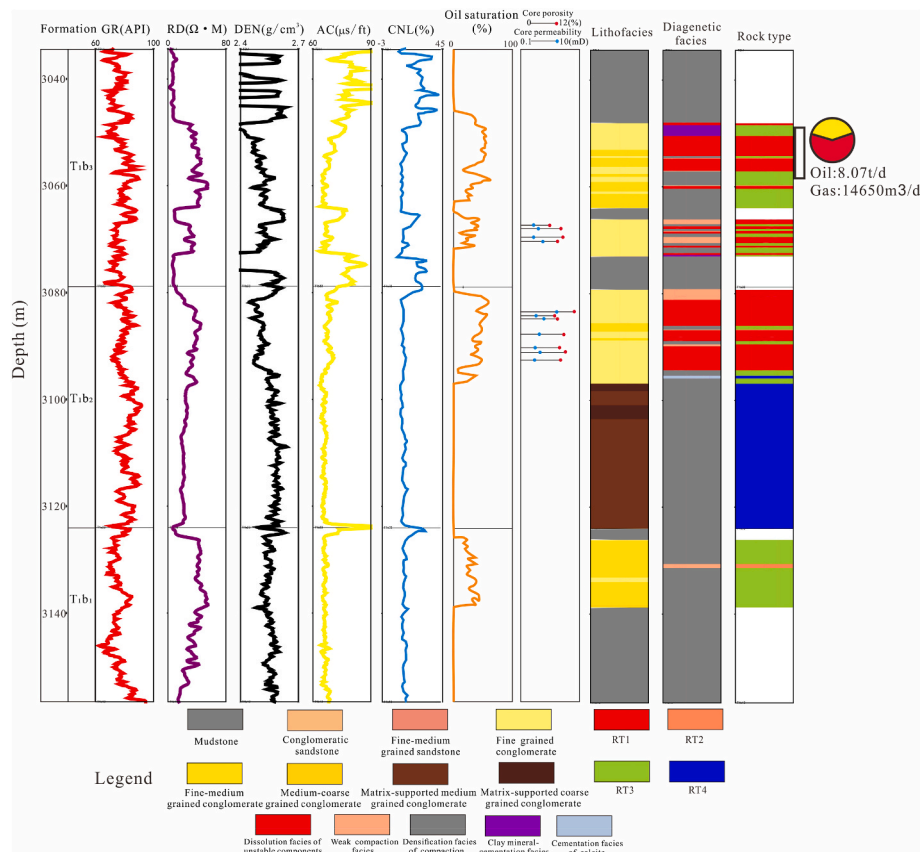
Fig. 14. Interpretation of rock type based on petrophysical facies of well MA15 in the Baikouquan Formation.

has obtained a high industrial oil flow, with oil production of 8.07 t/d, indicating that the evaluation method can serve as an effective tool for predicting favorable zones in the vertical direction of a single well.

4.4.2. Comparative analysis of cross section

The reservoir quality of the target layer is compared and analyzed parallel and perpendicular to the provenance direction (Figs. 15 and 16). It is unveiled that the reservoir quality of the Baikouquan Formation in the northern region is generally not high. Well XIA89 and XIA723 are basically dominated by RT3 and RT4, whereas RT1 and RT2 are less recorded. This is mainly because the close distance to the provenance has resulted in low structure maturity and poor sorting of conglomerate. In the middle area of T_1b_3 and sand group 1 of T_1b_2, the reservoir type is mainly RT2. The reservoir quality of the Baikouquan Formation reservoirs in well XIA94, MA154, and MA131 is relatively high, and they are typically featured by highly productive and stable oil flow (Fig. 15).

From west to east, the reservoir quality gradually gets better in T_1b_3, while sand group 1 of T_1b_2 owns the best reservoir quality in the middle part (Fig. 16). Due to the long transportation distance, the grain size of the conglomerate tends to be finer. When combined with constructive diagenetic reformation, high quality reservoirs could be formed. On the contrary, destructive diagenetic process could lead to porosity reduction and the development of RT3 and RT4. The rock type of sand group 2 of T_1b_2 is dominated by RT4. This is because during the deposition of sand group 2 of T_1b_2, the sedimentary facies are predominantly sandy debris flow where matrix-supported conglomerates are encountered.

In summary, sedimentary facies and lithofacies determine the interlayer heterogeneity of the reservoir, and the complex diagenetic reformation in the long geological history period has created intra-formational heterogeneity in the reservoir. It can be seen that the lateral ductility of reservoir type is relatively poor and reservoir quality varied greatly vertically, representing relatively strong interlayer and
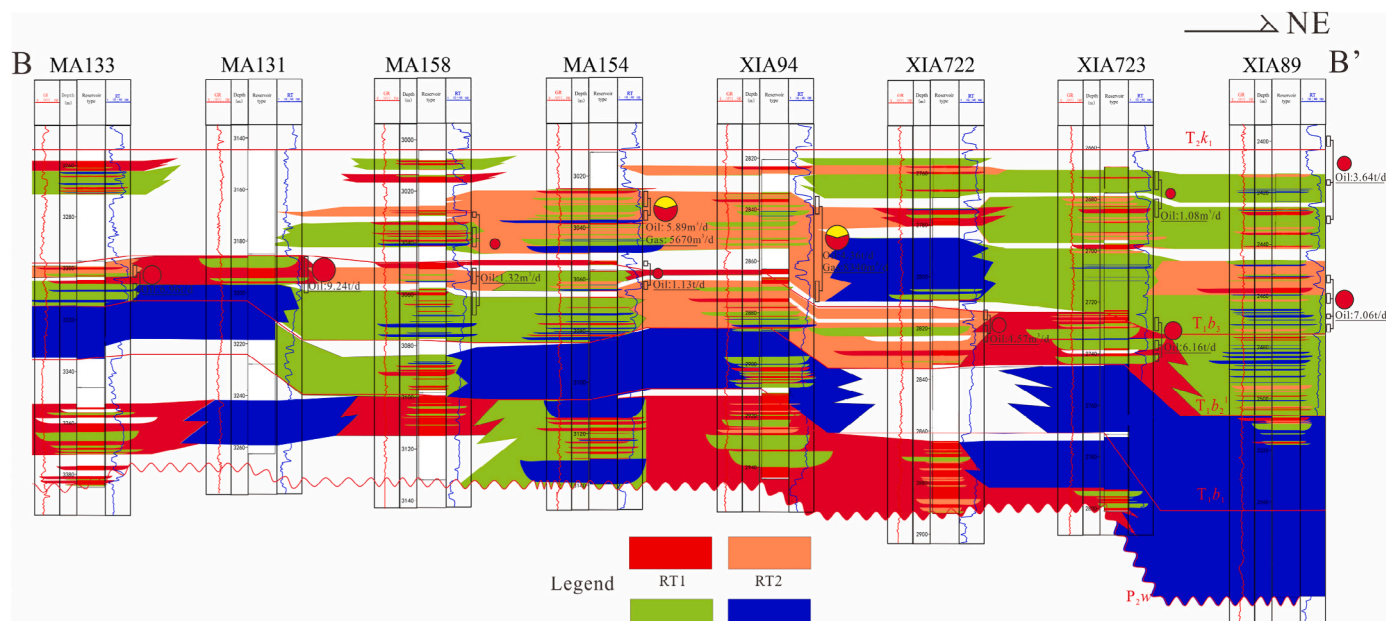
Fig. 15. Cross profile (B–B′) parallel the provenance direction showing the reservoir quality variation in the Baikouquan Formation. In the middle area, the rock type is mainly RT2. The location of the profile B–B′ can be seen in Fig. 1C.
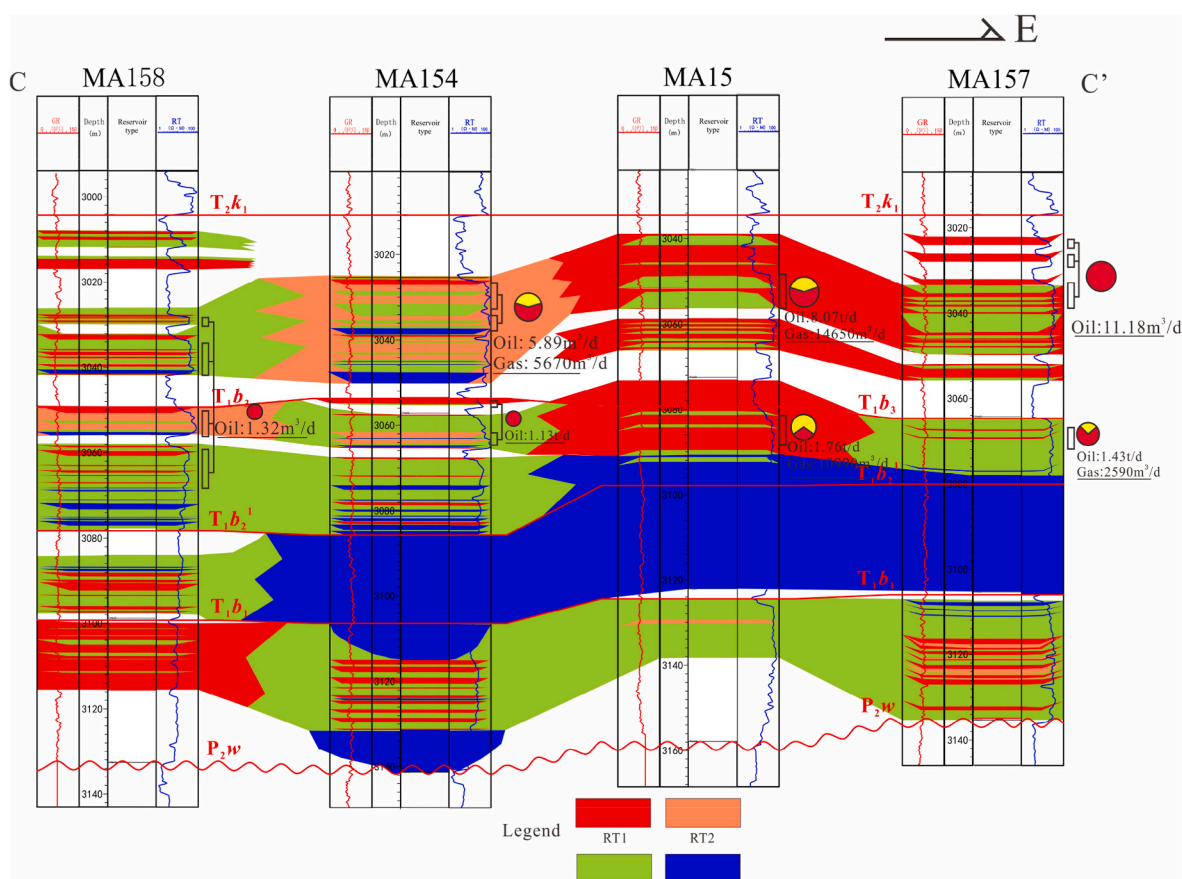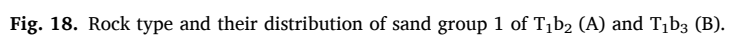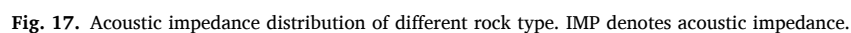

Fig. 16. Cross profile (C–C′) perpendicular to the provenance direction showing reservoir quality variation in the Baikouquan Formation. The location of the profile C–C′ can be seen in Fig. 1C.

intralayer heterogeneity of the reservoir, which conforms to the characteristics of typical low permeability oil reservoir.

4.4.3. Planar distribution of reservoir quality

The superposition of favorable lithofacies and diagenetic facies is the favorable petrophysical facies belt. Based on the aforementioned
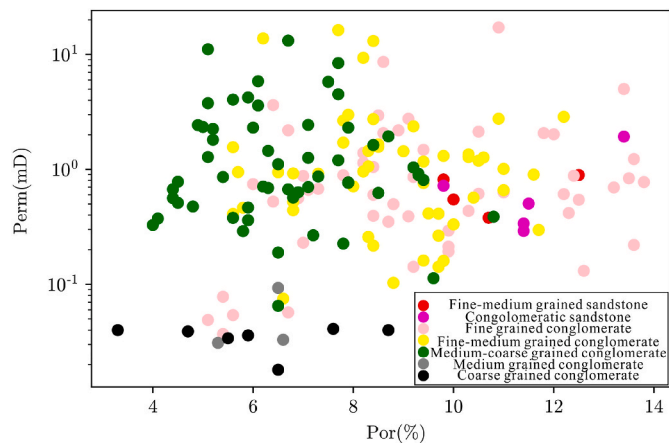
Fig. 17. Acoustic impedance distribution of different rock type. IMP denotes acoustic impedance.

Fig. 18. Rock type and their distribution of sand group 1 of T_1b_2 (A) and T_1b_3 (B).

Fig. 19. The Porosity–permeability crossplot for different lithofacies. RT1 are mainly fine grained conglomerate.
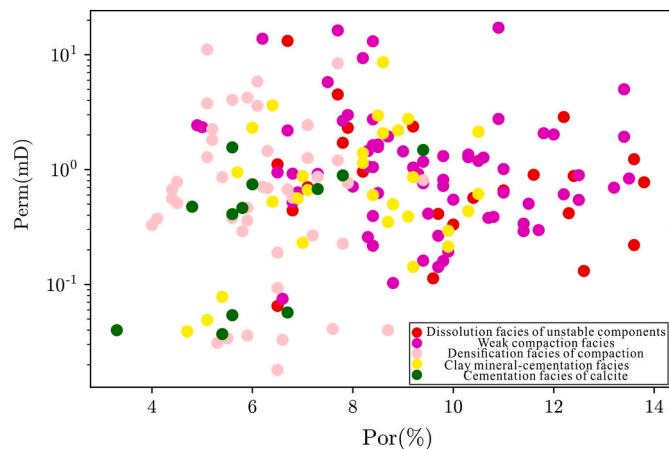

Fig. 20. The Porosity–osmosis crossplot for different diagenetic facies. RT2 and RT3 are predominantly controlled by dissolution and compaction.

division of rock type of each single well, the acoustic impedance of different rock types were counted. As shown in Fig. 17, the acoustic impedance within the Baikouquan Formation is utilized to validly differentiate different rock types. The acoustic impedance of RT1 was lower than 11,200 (g/cm³*m/s), while RT4 was generally greater than 11,800 (g/cm³*m/s). Additionally, acoustic impedance of RT2 and RT3 range from 11,000 to 11,600 (g/cm³*m/s), 11,600–11,800 (g/cm³*m/ s), respectively. Subsequently, the seismic acoustic impedance inversion

was performed to provide a foundation for the determination of different rock type boundaries. Eventually, the planar distribution maps of reservoir quality of main pay zone sand group 1 of T_1b_2 and T_1b_3 were forecasted (Fig. 18 A, B). The excellent reservoirs are obviously distributed in the middle and northeastern areas. Moreover, the middle area with fewer wells could be considered a pivotal region for further exploration and exploitation. All wells near favorable reservoirs have obtained industrial oil flow, which demonstrates the proposed method of screening the "sweet spot" in low permeability conglomerate reservoirs is feasible.

5. Discussion

5.1. The controlling factors of the variation in reservoir quality

During the deposition of the Baikouquan Formation, the paleotopographic slope is relatively gentle, creating favorable conditions for a wide coverage of fan-delta front and extension of the subaqueous distributary channel (Li et al., 2020; Zou et al., 2021). Among the same sedimentary microfacies (namely subaqueous distributary channel), different lithofacies and grain size caused by sediment gravity differentiation also exert a remarkable influence on the reservoir property. Lithological variation relates closely to the variation of reservoir property and porosity-permeability association. Cross plots between lithofacies, porosity, and permeability reveal that the fine-medium grained sandstones, conglomeratic sandstones, and fine grained conglomerates exhibit optimal porosity and permeability (Fig. 19). RT1 is dominated by fine grained conglomerates, whereas RT4 is primarily coarse grained conglomerates, indicating that RT1 and RT4 are primarily determined by grain size. In summary, the lithofacies offer the fundamental rock texture for the aperture evolution. Lithofacies with large particle sizes are easily packed with finer sediments, whereas lithofacies with fine particle sizes imply long-distance transportation with excellent reservoir quality.

Petrophysical facies with similar lithofacies will show distinct reservoir properties relying on the diagenetic facies. The diagenetic type exerts a straight impact on the aperture evolution which considerably affects the reservoir property and the porosity-permeability relationship. As shown in Fig. 20, dissolution could enlarge the pore space by ameliorating the aperture connection to reinforce the reservoir seepage capacity. However, most of the dissolution pores are intragranular thereby hardly improving the reservoir seepage capacity. Meanwhile, cementation can decrease the aperture space and result in minimized reservoir property. Weak compaction and dissolution are the principal constructive diagenesis in the Baikouquan Formation, while the other three destructive diagenesis would reduce the pore space. Weak compaction facies and dissolution facies are frequently observed in RT2 and RT3 are predominantly composed of densification facies of compaction.
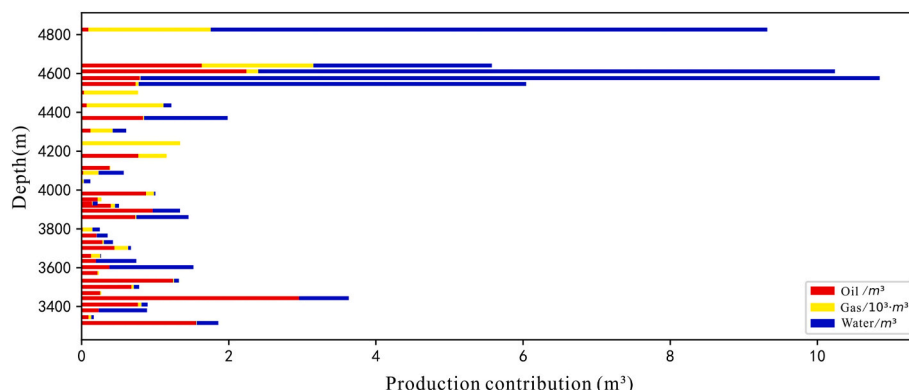

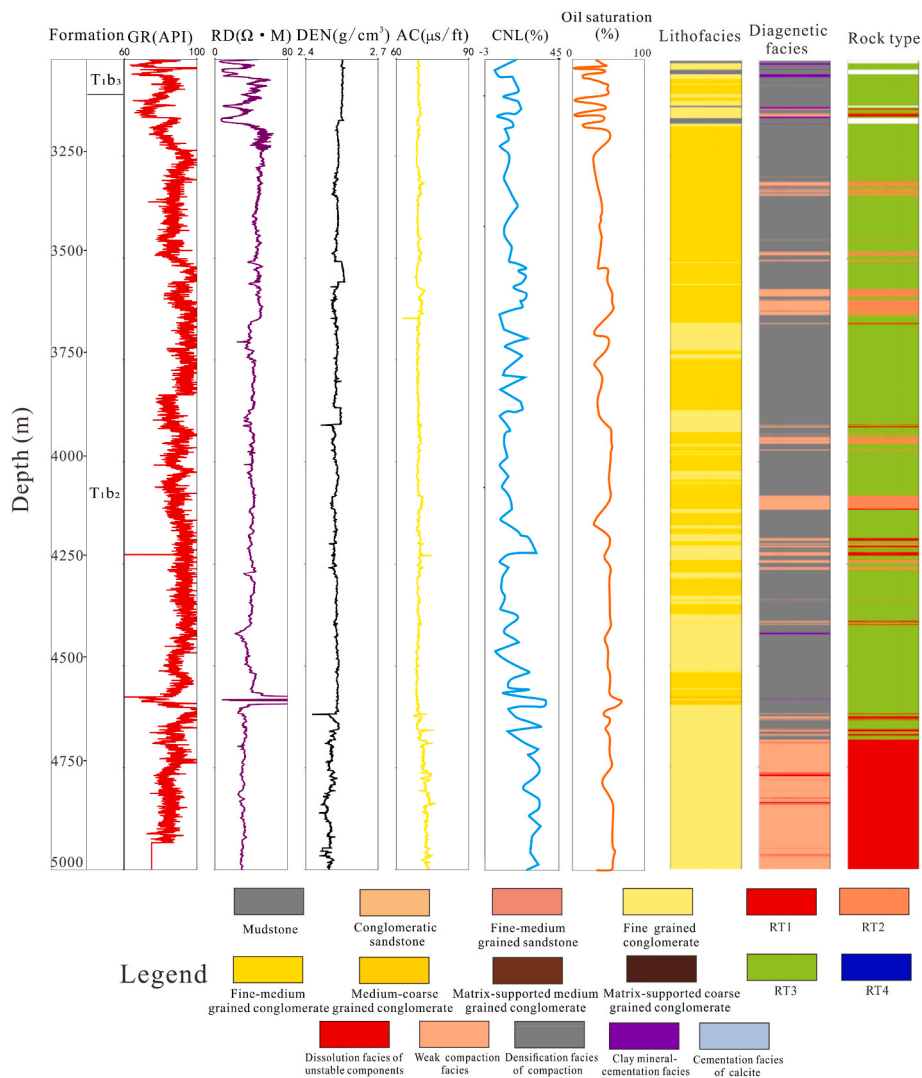**Fig. 21.** Fluid producing profile data of well MaHW1243.

Fig. 22. Reservoir evaluation of well MaHW1243. The fine-grained conglomerates and weak compaction correspond to main oil producing layers.

5.2. Reservoir evaluation with oil productivity

For the purpose of further evaluating the relationship between rock type and their productivity contribution characteristics, fluid producing profile logging was conducted to measure the oil, gas and water production of each fracturing section. The horizontal section of well MaHW1243 is divided into 27 sections for hydraulic fracturing. Based on the reservoir physical properties, water holdup, oil holdup and rotor speed (apparent speed), a total of 36 sets of monitoring data of production for each fracturing section is explained (seen in Fig. 21). The liquid production is 60.92 m^3/d (with water 40.21 m^3/d, oil 20.71 m^3/d) and the gas yield is 8312 m^3/d in total. The producing liquid mainly comes from the anterior and the posterior segments of fracturing sections 1-14. The 11th, 10th, 9th, 7th, 6th, and 1st-3rd fracturing sections are the main oil-producing layers, and the sum of these sections accounts for 85.80% of the total production. In this interval, the lithofacies are predominantly fine-grained conglomerates and the diagenetic facies are dominated by weak compaction, which are interpreted as RT1 and correspond well with fluid producing profile data (Fig. 22). The water production mainly comes from the well interval below 4535 m. There was no or very low production in the posterior fracturing sections and the reservoir type is mainly RT3.

6. Conclusions

We performed a study to evaluate low permeability conglomerate reservoirs using various data, such as cores, casting thin sections, and SEM data based on petrophysical facies. The conclusions drawn from the current research are stated below:

Generally, three lithofacies comprising conglomerates, sandstones, and mudstones are recognized, wherein conglomerates are the predominant type of lithofacies. Considering the granule size and clay content, the lithofacies were further divided into eight subtypes. The diagenetic facies in the Baikouquan Formation could be categorized mainly into five forms: weak compaction facies, dissolution facies of unstable components, clay mineral-cementation facies, cementation facies of calcite, and densification facies of compaction. A number of 12 petrophysical facies are identified by combining lithofacies and diagenetic facies. The clustering results of capillary pressure parameters with different petrogenesis units indicate that the rock type has a good relationship with R_{15}, which can determine the pore-throat structure. The distributional status of the optimal reservoir (RT1) and the worst reservoirs (RT4) are predominantly under the control of the lithofacies, whereas RT2 and RT3 are predominantly controlled by dissolution and compaction.

On the foundation of acoustic impedance, the reservoir quality distribution planar maps were drawn. The excellent reservoirs are

obviously distributed in the middle and northeastern areas. Moreover, the production test data obtained from 34 wells in the Baikoquan Formation validate the effectiveness of reservoir evaluation based on petrophysical facies. An evident positive association exists between the rock type and the single well production capacity. To sum up, the petrophysical facies method applies well in the reservoir evaluation of pore structure and the prediction of profitable porosity and permeability zones in ultra-low permeability conglomerate reservoirs of the Baikouquan Formation in Mahu oilfield due to the full consideration of the main geological factors affecting pore structure.

It is hard to obtain production without fracturing for this kind of unconventional reservoir. The formation of complex fracture network by reservoir fracturing requires favorable stress field conditions and rock fabric characteristics. It is easier to reproduce complex fracture network with smaller discrepancy between minimum and maximum horizontal stress, developed natural fractures, and higher brittleness index (Xu et al., 2019; Li et al., 2021). Unlike shale reservoir, coarse-grained conglomerate has distinct mechanical properties and fracturing mechanism. For instance, the core observation shows that the fracture is mainly developed around the gravel and its complexity is highly correlated to the grain size. It is highly recommended that future reservoir evaluation work must be focused on taking the parameter which is the main controlling factor of fracturing into consideration.

Author contribution

Zhichao Yu: Writing - original draft, Methodology, Software, Writing-review and editing. Zhizhang Wang: Project administration, Supervision. Qingping Jiang: Resources, Supervision. Jie Wang: Data curation, editing.: Yueli Feng: Investigation, Formal analysis. Jingrong Zheng: Formal analysis. Bestman Adjei Baffour: Editing.

Declaration of competing interest

The authors declare that they have no known competing financial interests or personal relationships that could have appeared to influence the work reported in this paper.

Data availability

The data that has been used is confidential.

Acknowledgements

References

Cao, Z., et al., 2018. Origin of different chlorite occurrences and their effects on tight clastic reservoir porosity. J. Petrol. Sci. Eng. 160, 384–392.

Daniel, A., Tarek, O.A., et al., 2022. Application of gradient boosting regression model for the evaluation of feature selection techniques in improving reservoir characterization predictions. J. Petrol. Sci. Eng. 208, 109244 https://doi.org/10.1016/j.petrol.2021.109244.

Fu, X., Wu, W., Hu, W., et al., 2022. A new method of gas reservoir evaluation based on neutron cross section logging. J. Petrol. Sci. Eng. 208, 109750 https://doi.org/10.1016/j.petrol.2021.109750.

Gao, S., Yi, Y., et al., 2021. Experimental research on inter-fracture asynchronous injection-production cycle for a horizontal well in a tight oil reservoir. J. Petrol. Sci. Eng. 208, 109647 https://doi.org/10.1016/j.petrol.2021.109647.

Guo, Y., 2021. Zou Caineng's "unconventional" road. Management Of State-owned Enterprise 48 (5), 1–12.

Hawkins, J.M., 2012. Petromation. Intergrated Formation Evaluation with Regression Analysis. SPE 574372.

Lei, D., Li, X., et al., 2021. Establishment and application of the optimized evaluation system for seismic exploration in Junggar Basin. Xinjing Pet. Geol. 42 (6), 720–725.

Li, C., Chen, G., Li, X., Zhou, Q., Sun, Z., 2021. The occurrence of tight oil in the Chang 8 lacustrine sandstone of the Huaqing area, Ordos Basin: insights into the content of adsorbed oil and its controlling factors. J. Nat. Gas GeoSci. 2468. https://doi.org/10.1016/j.jnggs.2021.11.001, 256X.

Li, G., Qin, J., Xian, C., et al., 2020. Theoretical understandings, key technologies and practices of tight conglomerate oilfield efficient development: a case study of the Mahu oilfield, Junggar Basin, NW China. Petrol. Explor. Dev. 47 (6), 1185–1197.

Lu, X., Dong, S., Xie, X., et al., 2019. Microfacies characteristics and reservoir potential of triassic Baikouquan Formation, northern Mahu sag, Junggar Basin, NW China. J. Nat. Gas GeoSci. 4 (1), 47–62. https://doi.org/10.1016/j.jnggs.2019.03.001.

Mehdi, M., Aydin, L., et al., 2021. On the evaluation of permeability of heterogeneous carbonate reservoirs using rigorous data-driven techniques. J. Petrol. Sci. Eng. 208, 109685 https://doi.org/10.1016/j.petrol.2021.109685.

Muhammad, A., Fang, O., et al., 2021. Fluid identification and effective fracture prediction based on frequency-dependent AVOAz inversion for fractured reservoirs. Petrol. Sci. 18 (4), 1069–1085. https://doi.org/10.1016/j.petsci.2021.07.011.

Obed, K., Cao, Q., Ye, J., 2021. Acoustic impedance and lithology-based reservoir porosity analysis using predictive machine learning algorithms. J. Petrol. Sci. Eng. 208, 109656 https://doi.org/10.1016/j.petrol.2021.109656.

Olmo, M., Javier, D., Francisco, J., et al., 2021. X-ray microtomography analysis to approach bioturbation's influence on minor-scale porosity distribution: a novel approach in contourite deposits. J. Petrol. Sci. Eng. 208 https://doi.org/10.1016/j.petrol.2021.109251.

Pan, S., Zheng, Z., et al., 2021. An optimized XGBoost method for predicting reservoir porosity using petrophysical logs. J. Petrol. Sci. Eng. 208 https://doi.org/10.1016/j.petrol.2021.109520.

Shan, X., Zou, Z.W., Meng, X.C., et al., 2016. Provenance analysis of triassic Baikouquan Formation in the area around Mahu depression, Junggar Basin. Acta Sedimentol. Sin. 34 (5), 930–939.

Shu Su, Y., Zha, M., Jiang, L., Ding, X., et al., 2022. Pore structure and fluid distribution of tight sandstone by the combined use of SEM, MICP and X-ray micro-CT. J. Petrol. Sci. Eng. 208 https://doi.org/10.1016/j.petrol.2021.109241.

Su, C., et al., 2021. Seismic description and fluid identification of thin reservoirs in Shengli Chengdao extra-shallow sea oilfield. Petrol. Explor. Dev. 48 (4), 889–899. https://doi.org/10.1016/S1876-3804(21)60074-5.

Tang, Y., Yin, T., Qin, J., et al., 2017. Development of large-scale shallow-water fan delta: sedimentary laboratory simulation and experiments. Xinjing Pet. Geol. 38 (3), 253–263.

Wang, X., Song, Y., Zheng, M., et al., 2021. Composite petroleum system and multi-stage hydrocarbon accumulation in Junggar Basin. China. Petrol. xploration 26 (4), 29–43.

Waqar, A., Murray, K., 2021. Integrating sedimentology and ichnology with rock typing and flow units: implications for clastic reservoir characterization. J. Petrol. Sci. Eng. 208 https://doi.org/10.1016/j.petrol.2021.109628.

Wu, Y., Pejman, T., Lin, C., et al., 2019. A comprehensive study on geometric, topological and fractal characterizations of pore systems in low-permeability reservoirs based on SEM, MICP, NMR, and X-ray CT experiments. Mar. Petrol. Geol. 103, 12–28. https://doi.org/10.1016/j.marpetgeo.2019.02.003.

Xie, L., You, Q., Wang, E., Li, T., Song, Y., 2022. Quantitative characterization of pore size and structural features in ultra-low permeability reservoirs based on X-ray computed tomography. J. Petrol. Sci. Eng. 208, 109733 https://doi.org/10.1016/j.petrol.2021.109733.

Xiong, Q., Peng, S., et al., 1994. A preliminary study of the new concept of petrophysical facies and its initial application in Lengdong-Leijia region in Liaohe Depression. Acta Pet. Sin. 15 (Suppl. I), 69–75.

Xiong, Q., Wang, Z., et al., 2010. Modern Reservoir Geology, Theory and Technology. Petroleum Industry Press, Beijing, pp. 63–70.

Xu, J., Li, J., Wu, Y., et al., 2019. Exploration and practice of volume fracturing technology in horizontal well of Mahu tight conglomerate reservoirs. China. Petrol. xploration 24 (2), 241–249.

Xue, Y., Cao, J., Wang, X., Du, H., 2022. Reservoir permeability estimation from seismic amplitudes using variational mode decomposition. J. Petrol. Sci. Eng. 208, 109293 https://doi.org/10.1016/j.petrol.2021.109293.

Yang, Z., Zou, C., Chen, J., et al., 2021. "Exploring petroleum inside or near the source kitchen": innovations in petroleum geology theory and reflections on hydrocarbon exploration in key fields. Acta Pet. Sin. 42 (10), 1310–1324.

Yu, Z., Wang, Z., et al., 2021. Volcanic lithology identification based on parameter-optimized GBDT algorithm: a case study in the Jilin Oilfield, Songliao Basin, NE China. J. Appl. Geophys. 194, 104443 https://doi.org/10.1016/j.jappgeo.2021.104443.

Yu, Z., Wang, Z., Wang, J., Li, Z., 2022. Subtle reservoirs and implications for hydrocarbon exploration in terrestrial lacustrine fan-delta deposits: insights from the Triassic Baikouquan Formation, Mahu Sag, Junggar Basin, western China. Mar. Petrol. Geol. 142, 105730 https://doi.org/10.1016/j.marpetgeo.2022.105730.

Zhang, K., Lin, N., Tian, G., et al., 2021. Unsupervised-learning based self-organizing neural network using multi-component seismic data: application to Xujiahe tight-sand gas reservoir in China. J. Petrol. Sci. Eng. 209, 109964 https://doi.org/10.1016/j.petrol.2021.109964.

Zou, Y., Shi, S., Zhang, S., et al., 2021. Experimental modeling of sanding fracturing and conductivity of propped fractures in conglomerate: a case study of tight conglomerate of Mahu sag in Junggar Basin, NW China. Petrol. Explor. Dev. 48 (6), 1383–1392. https://doi.org/10.1016/S1876-3804(21)60294-X.